Chemical Engineering Journal 414 (2021) 128761

Contents lists available at ScienceDirect

Chemical Engineering Journal

journal homepage: www.elsevier.com/locate/cej

# The efficient recovery of Au(III) ions from acidic solutions by a novel scavenger based on functionalized poly (styrene-*co*-maleimide) nanoparticles

Eugene Lakay [a], Sophie Hermans [b], Klaus Koch [a,1], Bert Klumperman [a,*]

[a] Department of Chemistry and Polymer Science, Stellenbosch University, Private Bag X1, Matieland, Stellenbosch 7602, South Africa
[b] IMCN Institute, Université catholique de Louvain (UCLouvain), Place L. Pasteur 1, 1348 Louvain-la-Neuve, Belgium

ARTICLE INFO

*Keywords:*
Poly(styrene-*co*-maleimide) nanoparticles
Scavenger
Au recovery
Au loading, metallic Au

ABSTRACT

Tertiary amine functionalized poly(styrene-*co*-maleimide) nanoparticles were readily synthesized by an organic solvent-free thermal imidization reaction. The obtained spherical nanoparticles, with average diameters of about 50 nm, were shown to be highly effective as a unique scavenger for the recovery of Au(III) ions from strong acidic solution. High equilibrium Au loading capacities (>570 mg/g) were obtained at 25 °C and the rate of metal ion uptake was remarkably fast. The Au(III) ions in the feed solutions were almost quantitatively recovered within 3–10 min, depending on the shaking speed during batch sorption. Elution of the adsorbed Au species was however incomplete with a maximum elution efficiency of 75% using acidified thiourea as eluant. XPS analysis showed that the adsorbed Au species were present as a mixture of Au(0), Au(I), and Au(III), which explained the inadequate elution. An alternative and innovative method to recover the adsorbed Au was developed consisting of digestion of the Au-loaded scavenger followed by reductive precipitation with water as reducing agent. The Au formerly loaded on the scavenger was successfully and completely recuperated as pure metallic Au. This is a step-change in the way Au is recovered from solution and eliminates the need for difficult, partial, and environmentally unfavorable elution processes of Au species strongly adsorbed on the scavenger particles.

## 1. Introduction

Over the years, South Africa's annual Au production has decreased significantly from around 1000 tonnes in 1970 to 90 tonnes in 2019 [1,2]. The steady fall in production is a consequence of a number of factors including declining ore grades, complex ore mineralogy, increased depth of mining which translates into higher costs involved in the mining operations. Although the supply of Au by South Africa has fallen, the worldwide demand for this precious metal has remained constant because of the enduring physical and chemical properties of Au and its widespread use in a range of important and technologically advanced applications [2–6]. Owing to dwindling primary resources and the economic value of the yellow metal, the recovery of Au from secondary sources, such as wastewaters, is gaining increasing importance [6–8]. Millions of cubic meters of wastewaters containing Au are generated annually by the electronic, jewelry, gold mining, and refining industries [6–10]. With the Au price recently surpassing all-time highs in US dollar terms and in most major global currencies, there is enormous incentive to recover Au(I/III) ions from wastewaters to generate revenue.

The Au concentration in wastewaters is often very low and needs to be upgraded to produce a higher-grade solution which can be treated to economically recover the metal. One way to achieve this is by loading the Au ions onto adsorbents and subsequently eluting the adsorbed Au species with a small volume of eluant solution. Much attention has been paid to the recovery of Au(III) from solution with different types of adsorbents [6–13]. In some of these cases, very high Au loadings were obtained [8,9]. The major challenge, however, is to completely elute the adsorbed Au species from the adsorbent to generate a concentrated Au-bearing stream for further processing. This is not a trivial task since Au species are known to bind strongly to many adsorbents which result in losses. To elute adsorbed Au species from adsorbents with some degree of success, strongly acidic solutions or acidified thiourea solutions are required [6,7,13–15]. From a practical standpoint, this is very

* Corresponding author.
*E-mail address:* bklump@sun.ac.za (B. Klumperman).
[1] Prof Klaus Koch, who acted as the PhD supervisor for Dr Eugene Lakay, sadly passed away on 2 January 2020.

https://doi.org/10.1016/j.cej.2021.128761
Received 17 September 2020; Received in revised form 23 January 2021; Accepted 26 January 2021
Available online 1 February 2021
1385-8947/© 2021 Elsevier B.V. All rights reserved.

expensive, hazardous, and not environmentally friendly [16]. Also, the downstream processing to recover eluted Au species from spent thiourea solution by refining to a final Au product is not established. This limits the use of acidified thiourea solution as an eluant in industrial applications, and although reasonably effective, the reagent is of academic interest only at this stage. Other options could be to precipitate the eluted Au species from the spent thiourea eluant solution or to incinerate the Au-loaded adsorbent to recover the Au. But this will generate contaminated Au-rich residues requiring additional processing which adds another layer of cost and complexity. It is therefore not sufficient to merely adsorb Au(III) onto an adsorbent and making use of impractical methods to partially elute the metal ions. Also in literature, rarely any emphasis is placed on the Au upgrade ratio achieved by the adsorption-elution process. The shortcomings mentioned above represent an opportunity to develop an alternative process to bypass the limitations often associated with elution processes of loaded Au from adsorbents. To contribute to the existing body of knowledge on this subject matter and to bridge the gap in the scientific literature, the aim of our study was to manufacture a novel scavenger, capable of achieving reasonably high Au loading capacities, but also from which the adsorbed Au species can be effortlessly and completely recovered as a pure Au product, without the need for difficult and costly elution processes. To accomplish these ambitious objectives, suitably functionalized poly(styrene-*co*-maleimide) nanoparticles were identified as an appropriate scavenger. The scavenger nanoparticles offer several important characteristics such as large surface-area-to-volume ratio, very good sorption ability and reactiveness due to the amine functional groups, and resistance against degradation by acidic chloride solutions which is typically the medium for industrial precious metal waste liquors. The choice of polymer matrix for our scavenger stems from the fact that (1) the high reactivity of the maleic anhydride moieties in poly(styrene-*co*-maleic anhydride) toward nucleophilic reagents enables the straightforward and reproducible synthesis of a variety of functionalized maleimide nanoparticles, (2) the starting materials are cheap and readily available, which means the Au-loaded scavenger material can be entirely disintegrated to recover the metal value.

Poly(styrene-*co*-maleimide) derivatives and nanoparticles have been widely studied for various applications. Ahokas and Samyn synthesized poly(styrene-*co*-maleimide) nanoparticles for utilization in paper coatings [17,18]. In both cases, the nanoparticles were prepared by thermal imidization of poly(styrene-*co*-maleic anhydride) with ammonia as the imidization agent. Interestingly, *N*-substituted poly(styrene-*co*-maleimide) has also found use in catalysis. For example, in a recent paper, the maleimide polymer was prepared by modification of the maleic anhydride polymer with 3-aminopyridine. Zinc chloride was immobilized onto the polymer as nanoparticles and successfully tested as a catalyst in the regioselective synthesis of 1,4-disubstituted 1,2,3-triazole [19]. Previous work in our research group also demonstrated the versatility of *N*-substituted poly(styrene-*co*-maleimide) particles which were shown to possess antibacterial and antifungal properties [20].

In this work, poly(styrene-*co*-maleimide) nanoparticles with a tertiary-amine functionality were prepared by thermal imidization of the corresponding maleic anhydride co-polymer precursor with 3-*N*,*N*-dimethylaminopropyl-1-amine using water as the reaction medium. The amine-functionalized nanoparticles were effortlessly isolated from the water-based, stable polymer dispersion and used as a scavenger for the recovery of Au(III) ions from acidic solutions. Most notably, the adsorbed Au species were quantitatively recovered from the Au-loaded scavenger as metallic Au flakes, without elution processes. This is a step-change in the recovery of Au(III) ions from solution. The targeted application is Au(III) recovery from highly acidic, industrial effluents containing anionic Au(III) chloro-complexes ($AuCl_4^-$). To the best of our knowledge, the use of *N*-substituted poly(styrene-*co*-maleimide) nanoparticles as a scavenger for Au(III) recovery or any other metal ion has not yet been reported in the scientific literature.

## 2. Materials and methods

### 2.1. Materials

Poly(styrene-*co*-maleic anhydride) pellets (roughly 0.3 × 0.8 cm) (hereafter denoted as PSMA) with a weight average molar mass of 80 × $10^3$ g/mol and a composition of 26 wt% maleic anhydride was donated by Polyscope Polymers BV (Geleen, the Netherlands). Analytical grade 3-*N*,*N*-dimethylaminopropyl-1-amine (DMAPA) was purchased from Sigma-Aldrich. High purity deionized water (Millipore Milli-Q, 18 MΩ cm) was used throughout this work. All other chemicals were of analytical-grade and used without further purification. For Au(III) recovery experiments, synthetic feed solutions were prepared from $NaAuCl_4{\cdot}2H_2O$ salt (Sigma Aldrich) in 2 M HCl solutions. For the mixed-metal recovery experiments, synthetic feed solutions were prepared from the following salts (Sigma Aldrich): $NaAuCl_4{\cdot}2H_2O$, $Na_2PdCl_4$, $Na_2PtCl_6{\cdot}6H_2O$, $Na_2IrCl_6{\cdot}6H_2O$, $Na_3RhCl_6$, $NiCl_2{\cdot}6H_2O$, $CuCl_2{\cdot}2H_2O$, $FeCl_2{\cdot}xH_2O$, $PbCl_2$, $MnCl_2$, and $MgCl_2$.

### 2.2. Methods

Particle size and morphology were determined by Transmission Electron Microscopy (TEM), using a JEM 1200EXII model (JEOL, Japan) microscope. An accelerating voltage of 200 kV was used throughout the analysis. A drop of the water-based, stable PSMI dispersion was placed on a carbon-coated 200 mesh copper grid, followed by drying at ambient conditions before it was attached to the sample holder on the microscope. Prior to use, the grids were glow discharged for 30 s under air in a vacuum of $10^{-2}$ mbar. Particle size and morphology of the nanoparticles, in the solid-state, were determined on a nano-scale resolution with Scanning Electron Microscopy (SEM), using a Nova™ NanoSEM 430 microscope (FEI Company). The particle size distributions and average particle diameters were determined with statistical analysis and by measuring 300–400 individual particles from various micrographs using *Image J*, a public domain image processing program [21]. Elemental analysis was done with an Exeter Analytical CE440 elemental analyzer. Carbon-13 Nuclear Magnetic Resonance ($^{13}$C NMR) spectra were recorded on a Varian Inova 600 MHz spectrometer operating at 150.586 MHz. A typical sample consisted of 250 mg polymer dissolved in 1 mL acetone-$d_6$ and the analysis was conducted at an elevated temperature of 44.8 °C. All samples were carefully filtered before spectroscopic measurement. $^{13}$C NMR resonances were assigned in conjunction with APT and DEPT techniques. Fourier transform infrared (FTIR) spectra were recorded on a Nexus FTIR spectrophotometer equipped with a Smart Golden Gate attenuated total reflectance (ATR) diamond from Thermo Nicolet, with ZnSe lenses. Each spectrum was scanned 32 times with 4 $cm^{-1}$ resolution and data analysis was performed with Omnic Software version 7.2. Surface area measurements were carried out using the Brunauer-Emmet-Teller (BET) method on a Micrometrics ASAP 2010 (Accelerated Surface Area and Porosity) apparatus using nitrogen as adsorbent. The samples were degassed at 100 °C for approximately 24 h before use. Each degassed sample (0.1–0.4 g) was weighed accurately to four decimal places and placed in a sample tube. The analysis was performed using an automatic multi-point adsorption program, measuring the volume of nitrogen adsorbed by the sample at a range of $N_2$ pressures. Powder X-ray diffraction (PXRD) analysis was conducted with a Siemens D8 Advance diffractometer using Cu $K_\alpha$ radiation ($\lambda = 1.540$ Å) operated at 40 kV and 30 mA. PXRD patterns were recorded in the range 10–80° (2θ) with a scan step of 0.02° using a prolonged irradiation exposure time of 3 h. X-ray photoelectron spectroscopy (XPS) analyses were performed on a Kratos Axis Ultra spectrometer (Kratos Analytical, Manchester, UK) equipped with a monochromatized aluminum X-ray source (powered at 10 mA and 15 kV). The sample powders were pressed onto double-sided adhesive tape mounted on polymer plates fixed on the multi specimen holder. The pressure in the analysis chamber was about $10^{-6}$ Pa. The

angle between the normal to the sample surface and the direction of photoelectrons collection was about 0°. Analyses were performed in the hybrid lens mode, with the resulting analyzed area of 700 μm × 300 μm. The pass energy was set at 160 eV for the survey scan and 40 eV for narrow scans. In the latter conditions, the full width at half maximum (FWHM) of the Ag $3d_{5/2}$ peak of a standard silver sample was about 0.9 eV. Charge stabilization was achieved by using the Kratos Axis device. The following sequence of spectra was recorded: survey spectrum, C1s, O1s, N1s, Cl 2p, Au 4f, and C1s again to check for charge stability as a function of time and the absence of degradation of the sample during the analyses. The C1s peak of carbon was fixed at 284.8 eV to set the binding energy scale. Spectra were deconvoluted with the CasaXPS program (Casa Software Ltd., UK) with a Gaussian/Lorentzian (70/30) product function and after subtraction of a linear baseline. Molar fractions were calculated using peak areas normalized based on acquisition parameters, experimental sensitivity factors, and transmission factors provided by the instrument manufacturer.

For the batch adsorption tests, a horizontal mechanical shaker (Labcon, BR-30L) was used for agitation of the metal-bearing feed solutions with the PSMI scavenger material for specified contact times. Unless otherwise stated, the shaking speed of the shaker was 250 rpm. Most adsorption tests were repeated at least three times, and results were reproducible with negligible differences. A Mars microwave digester was used to digest Au-loaded scavenger samples for mass balance purposes and for Au recovery by precipitation. The concentration of the metal ions in the feed solutions and barren solutions (liquors obtained after Au(III) recovery and filtration) were determined by Inductively Coupled Plasma Optical Emission Spectrometry, ICP-OES (SPECTRO Arcos), using a linear calibration method. Standards were matrix matched to acid concentrations of the samples. After calibration and quality check analysis to verify the accuracy of standards, samples were analyzed.

### 2.3. Synthesis of functionalized poly(styrene-co-maleimide) nanoparticles

Poly(styrene-*co*-(*N*-(3-*N*',*N*'-dimethylaminopropyl)-maleimide)) nanoparticles (denoted as PSMI hereafter) were synthesized by thermal imidization of poly(styrene-*co*-maleic anhydride) (PSMA) with 3-*N*,*N*-dimethylaminopropyl-1-amine (DMAPA) in a Büchi double-walled oil-heated autoclave equipped with a mechanical agitator using water as a solvent. A typical preparation was as follows: 2 × 835 μL DMAPA was added to 5 g PSMA (1:1 molar ratio between primary amine and maleic anhydride moieties) suspended in 50 mL $H_2O$ and allowed to stir at 1000 rpm for 6 h at a temperature of 150–180 °C and pressure of 5–7 bar. The imidization reaction illustrating the modification of PSMA into the corresponding amine-functionalized PSMI derivative is as shown in Scheme 1.

During the imidization reaction, the commercial PSMA copolymer pellets dissolved and after a certain residence time (6 h), at elevated temperature (>150 °C) and pressure (>5 bar), a stable, opaque, water-based dispersion formed containing the functionalized PSMI nanoparticles (refer to the supplementary information section for photographs of the starting PSMA copolymer and the formed PSMI dispersion). The polymer dispersion was purified by dialysis for at least 48 h using dialysis tubing with a molecular weight cut-off of 3500 g/mol. The functionalized PSMI nanoparticles were isolated from the dispersion by freeze-drying for at least 18 h. Subsequently, the resulting off-white fine powdered substance was dried at 50 °C in vacuo (200 mbar) for 6–8 h to constant weight before used as a scavenger adsorbent material in the Au(III) recovery experiments.

### 2.4. Adsorption and elution experiments

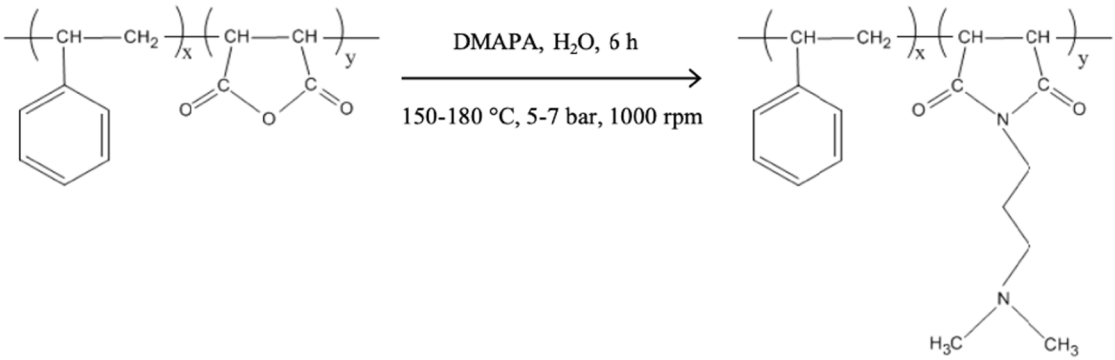
#### 2.4.1. Equilibrium adsorption isotherm

A thirteen-point equilibrium adsorption isotherm for Au(III) ions, at various scavenger-to-feed solution ratios, was generated for the PSMI scavenger material. Scavenger samples were contacted with a 911 mg/L Au(III) synthetic feed solution in individual 20 mL glass stoppered containers at ambient temperature for 24 h to ensure that equilibrium was reached. The Au(III) feed solution matrix was 2 M HCl. Ultra-violet visible (UV–Vis) spectroscopy indicated that the Au(III) ions in the feed solutions were present as stable anionic tetrachloroaurate complexes, or $[AuCl_4]^-$ ions [22]. The scavenger-to-feed solution ratios are shown in Table 1.

Upon completion of the batch adsorption tests, the Au-loaded scavengers were effortlessly and efficiently separated from the barren solutions by centrifugation at 4500 rpm for 15–20 s. The barren solutions were subsequently filtered (0.2 μm PTFE syringe filters, PALL) and analyzed for residual Au(III) with ICP-OES. The amount of Au loaded per unit mass of scavenger was determined by Eq. (1) and the percentage of Au recovery was calculated by Eq. (2) [11,23]:

**Table 1**
Scavenger-to-feed solution ratios used for the generation of Au(III) adsorption isotherms.

| Adsorption point | Scavenger mass (mg) | Feed solution (mL) | Scavenger-to-solution ratio (mg/mL) |
|---|---|---|---|
| 1 | 5 | 10 | 0.5 |
| 2 | 10 | 10 | 1 |
| 3 | 20 | 10 | 2 |
| 4 | 30 | 10 | 3 |
| 5 | 40 | 10 | 4 |
| 6 | 50 | 10 | 5 |
| 7 | 80 | 10 | 8 |
| 8 | 100 | 10 | 10 |
| 9 | 120 | 10 | 12 |
| 10 | 150 | 10 | 15 |
| 11 | 200 | 10 | 20 |
| 12 | 250 | 10 | 25 |
| 13 | 300 | 10 | 30 |




**Scheme 1.** Chemical modification of PSMA into PSMI during the thermal imidization reaction in water with 3-*N*,*N*-dimethylaminopropyl-1-amine (DMAPA).

$$Q_e = (C_0 - C_e)\ V/m \quad (1)$$

$$\text{Recovery (\% (m/m))} = ((C_0 - C_e)/C_0) \times 100\% \quad (2)$$

where $Q_e$ (mg/g) is the equilibrium Au adsorption on the scavenger, $C_0$ and $C_e$ (mg/L) are the initial and equilibrium concentrations of Au (III) in the feed and barren solutions, respectively. $V$ (L) is the volume of the sample feed solution and $m$ (g) is the mass of the scavenger sample.

Four adsorption isotherm models, namely Langmuir, Freundlich, Redlich-Peterson and the Sips models were fitted to the experimental adsorption data points [23–26]. The models were fitted by non-linear least squares regression analysis using the Solver function in Microsoft Excel. To determine the validity of the fitted isotherm models, the correlation coefficient ($R^2$) was determined by Eq. (3) [24,26]:

$$R^2 = 1 - \frac{\sum_{n=1}^{n}\left(Q_{exp.n} - Q_{model.n}\right)^2}{\sum_{n=1}^{n}\left(Q_{exp.n} - \overline{Q_{exp.n}}\right)^2} \quad (3)$$

where $n$ is the number of experimental data points, $Q_{exp}$ is the experimental adsorption data points and $Q_{model}$ is the calculated adsorption of Au(III) onto the PSMI scavenger according to the model equations.

Baseline Au(III) adsorption tests were also conducted with pulverized virgin PSMA, at solid-to-feed solution ratios of 1, 5, and 20. None of the Au(III) ions in the 731 mg/L Au(III) feed solution was recovered and the color of the virgin polymer remained unchanged, indicating that the unmodified PSMA polymer, with maleic anhydride groups, had no affinity towards Au(III) ions. This indicated that functionalization is required to extract the Au(III) ions from solution.

### 2.4.2. Adsorption kinetics

To determine the rate of Au(III) adsorption, approximately 50 mg samples of the scavenger were contacted with 10 mL aliquots of a 208 mg/L Au(III) feed solution for 0–15 min. Kinetic studies were performed with the batch conditions and analysis as described above except for shorter contact times. The amount of Au loaded onto the scavenger was calculated by Eq. (4):

$$Q_t = (C_0 - C_t)\ V/m \quad (4)$$

where $Q_t$ (mg/g) is the Au species adsorption on the scavenger at time $t$, $C_0$ is the initial Au(III) concentration in the feed solution and $C_t$ (mg/L) is the concentration of Au(III) in the barren solution at time $t$. $V$ (L) is the volume of the sample solution and $m$ (g) is the mass of the scavenger sample. The effect of different shaking speeds, during the batch sorption, on Au(III) uptake by the scavenger (50, 150 and 250 rpm) was determined.

### 2.4.3. Adsorption thermodynamics

The effect of temperature on the adsorption of Au(III) ions onto the scavenger was evaluated at 10, 20, 25, and 40 °C to determine the thermodynamic parameters. Four 10 mL aliquots of Au(III) feed solution were transferred into sealed 25 mL Schott bottles and inserted into a water bath set to the targeted temperatures. In all cases, the concentration of Au(III) in the feed solutions was 212 mg/L in a 2 M HCl matrix. Once the individual temperatures had been reached, 50 mg samples of scavenger were added to the Schott bottles and subsequently shaken in a thermostated shaker at 250 rpm for 5 min, after which the barren solutions were isolated from the Au-loaded scavengers and analyzed as described previously. The three fundamental thermodynamic parameters, namely, Gibbs free energy ($\Delta G^0$), enthalpy change ($\Delta H^0$), and entropy change ($\Delta S^0$) were calculated using the following set of equations [27–29]:

$$\Delta G^0_{ads} = -RT \ln K_c \quad (5)$$

The relationship between $\Delta G^0_{ads}$, $\Delta H^0_{ads}$, and $\Delta S^0_{ads}$ is described as:

$$\Delta G^0_{ads} = \Delta H^0_{ads} - T\Delta S^0_{ads} \quad (6)$$

The classical van't Hoff equation is obtained by substituting Eq. (5) into Eq. (6):

$$\ln K_c = -\Delta H^0_{ads}/RT + \Delta S^0_{ads}/R \quad (7)$$

where $R$ is the universal gas constant (8.314 J/mol/K), $T$ is the absolute temperature in Kelvin (K), and $K_c$ is the equilibrium constant, which was determined by Eq. (8):

$$K_c = C_{SP,e}/C_e = (C_0 - C_e)/C_e \quad (8)$$

where $C_e$ and $C_{SP,e}$ are the equilibrium concentration in solution (mg/L) and the solid phase concentration at equilibrium (mg/L), respectively. The equilibrium constant is dimensionless.

### 2.4.4. Elution behavior

Elution experiments were conducted to determine the elution efficiency of adsorbed Au species from the Au-loaded scavengers. In a typical elution experiment, 10 mL of eluant solution was contacted with approximately 50 mg of Au-loaded scavenger for 24 h. The elution studies were performed with the batch conditions and analysis as described previously. Table 2 shows the list of eluants, and the Au loadings achieved on the scavengers, used in the elution experiments.

In elution test 1 (denoted as **EI**), for example, Au(III) ions were loaded onto an adequate amount of scavenger from a feed solution of Au (III) in a 2 M HCl matrix. The Au(III) ions initially in the feed solution were adsorbed onto the scavenger with a resulting Au loading of 32 mg/g. The adsorbed Au species were then eluted from the Au-loaded scavenger with a 3 M HCl solution. Prior to conducting the elution tests, the scavengers pre-loaded with Au(III) were washed with 0.5 M HCl solution (×3) immediately after adsorption to remove any entrained Au(III) solution.

The percentage of elution was determined by Eq. (9):

$$\text{Elution (\% (m/m))} = ((C_{aq}/Q_{ads})\ V/m) \times 100\% \quad (9)$$

where $C_{aq}$ (mg/L) is the concentration of Au species in the eluate solution, $Q_{ads}$ (mg/g) is the amount of Au adsorbed on the scavenger, $V$ (L) is the volume of the sample eluate solution and $m$ (g) is the mass of the Au-loaded scavenger sample.

### 2.4.5. Metallic Au recovery from Au-loaded scavenger and mass balancing

In these experiments, 50 mg of Au-loaded scavengers were suspended in 100 mL $HNO_3$ solution (10% (v/v), Suprapur® quality) and digested in a microwave for 30 min at a temperature of 230 °C and pressure of 600 psi. The completely digested, opaque suspension was cooled to ambient temperature and then filtered (0.45 μm cellulose nitrate filter paper, Sartorius) using a Milli-pore filtration set-up to remove any suspended matter from the solution. Deionized water (~100 mL) was subsequently added to the yellow-colored supernatant solution which resulted in the spontaneous sedimentation of metallic, micron-sized Au flakes. The metallic Au flakes were thoroughly washed with deionized water and allowed to dry under ambient conditions overnight. The supernatant solution after Au sedimentation, now colorless, was analyzed for trace amounts of aqueous Au species, and the mass of the

**Table 2**
Eluants used for the elution of adsorbed Au species from the Au-loaded scavengers.

| Elution test | Eluant solution | Au(III) loading[†] |
|---|---|---|
| **EI** | 3 M HCl | 32 mg/g |
| **EII** | 6 M HCl | 32 mg/g |
| **EIII** | 3 M $HNO_3$/0.5 M HCl | 50 mg/g |
| **EIV** | 6 M $HNO_3$/0.5 M HCl | 50 mg/g |
| **EV** | 0.25 M Thiourea/2 M HCl | 82 mg/g |

[†] Au loading onto the scavenger. In all cases, Au(III) recovery from the feed solutions were > 99%.

metallic Au precipitate was recorded. An elemental mass balance for Au was performed around the digestion and Au precipitation stages (Scheme 2) and by using Eq. (10):

$$\text{Mass balance accountability } (\%) = (\textit{mass of Au out/mass of Au in}) \times 100\% \quad (10)$$

where *mass of Au in* is the total mass (g) of Au that went in with the Au-loaded scavenger, and *mass of Au out* is the total mass (g) of Au in the sedimented metallic Au, plus the mass (g) of residual Au species in the supernatant solution (after Au sedimentation).

#### 2.4.6. Competitive adsorption behavior

Metal recovery tests were carried out from mixed-metal solutions containing Au(III) ions, platinum group metal (PGM) ions, and other heavy metal ions. Firstly, 50 mg samples of scavenger were contacted with a feed solution containing 21 mg/L Au(III) and ~ 50 mg/L Pd(II), Rh(III), Ir(IV), and Pt(IV) in a 2 M HCl matrix. Secondly, 50 mg samples of the scavenger were contacted with a feed solution containing 143 mg/L Au(III) and ~ 300 mg/L Ni(II), Cu(II), Fe(II), Pb(II), Mg (II), and Mn(II) in a 2 M HCl matrix. The Au-bearing feed liquors were prepared in such a way so that the concentrations of the co-existing metal ions were at least twice the concentration of Au(III) ions in solution to ensure a highly competitive environment during adsorption. Lastly, a series of Au(III) recovery tests were performed in the presence of different concentrations of HCl and common counter anions, including chloride, nitrate and sulphate. The metal uptake experiments were performed with the batch conditions and analysis described previously.

## 3. Results and discussion

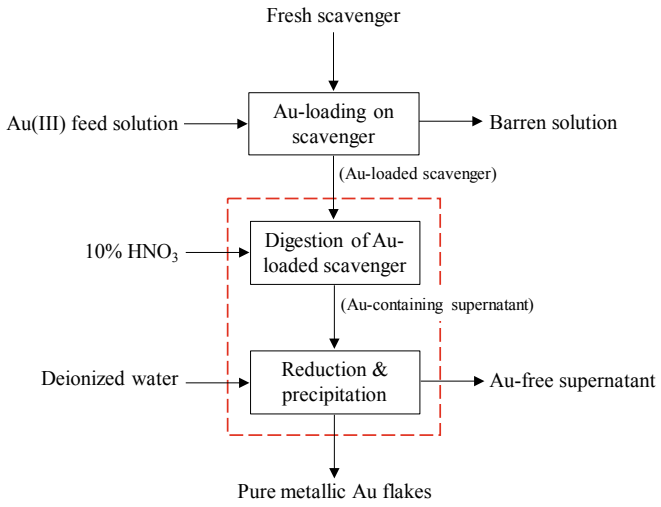
The prepared functionalized poly(styrene-co-maleimide) (PSMI) nanoparticles, as described in Section 2.3, were meticulously characterized and subsequently used as a new scavenger for the efficient recovery of Au(III) ions from acidic solutions.

### 3.1. Characterization of PSMI nanoparticles

#### 3.1.1. Elemental analysis

The elemental analyses of PSMA and PSMI are shown in Table 3. The values for C, H, and N are the actual microanalytical data and the calculated values are given in parentheses. The O content was calculated by difference.

Table 3 shows that there is an excellent correlation between experimental and calculated values for the C, H, and N elements. As expected,




**Scheme 2.** Block-flow diagram illustrating the Au recovery process from solution to metal.

**Table 3**
Elemental analyses (wt. %) of virgin PSMA and functionalized PSMI polymers.

| Material | % C (calc) | % H (calc) | % O (calc)[a] | % N (calc) |
|---|---|---|---|---|
| PSMA | 80.4 (81.0) | 6.4 (6.3) | 13.3 (12.7) | – [b] |
| PSMI | 78.7 (79.3) | 7.7 (7.7) | 7.5 (6.9) | 6.1 (6.1) |

[a] Oxygen content (%) = 100% - ∑ (% C, % H, % N).
[b] Experimental and calculated values were zero.

apart from O, the PSMA polymer consisted of C and H only, whilst the PSMI derivative contained C, H, and N elements. This confirmed successful conversion from PSMA into PSMI during the imidization reaction (Scheme 1). Moreover, the results indicated that complete conversion of PSMA into the PSMI derivative was obtained based on the identical experimentally observed and calculated values for nitrogen.

#### 3.1.2. Analysis by $^{13}C$ NMR

Shown in Fig. 1 are the $^{13}C$ NMR spectra of PSMA and PSMI, respectively.

A downfield chemical shift (δ) of carbonyl carbons (C5 and C6) from $\delta_{PSMA}$ ($^{13}C$) = 173 ppm to $\delta_{PSMI}$ ($^{13}C$) = 180 ppm occurred after conversion of PSMA into PSMI. The absence of the carbonyl carbon peaks associated with the maleic anhydride moiety of PSMA in the spectrum of PSMI confirmed that complete conversion occurred from the maleic anhydride into the maleimide derivative. Amine functionalization is further proven by the appearance of DMAPA carbons C7-C11 in the spectrum of PSMI. As expected, no chemical shift changes were observed for the styrene carbons (C12-C15) between 125 and 132 ppm because of the modification. Interestingly, the quaternary carbon of the styrene unit (C12) showed multiple peaks which can be ascribed to stereochemical configurations and copolymer sequences [30,31]. The carbon peaks (C1-C4 and C7-C11) were unambiguously assigned in conjunction with an attached proton (APT) test and distortionless enhancement by polarization transfer (DEPT) experiment (refer to Fig. S3 in the supplementary information section for the $^{13}C$ NMR APT spectrum).

#### 3.1.3. FTIR analysis

Fig. 2 shows the FTIR spectra of virgin PSMA and PSMI in the 1400–2000 $cm^{-1}$ region.

The characteristic C = O stretching vibrations associated with maleic anhydride groups of PSMA are easily distinguished from the C = O stretching vibrations of the PSMI maleimide groups. A clear shift in the C = O absorption bands from 1851 and 1772 $cm^{-1}$ (maleic anhydride group in the five-membered ring) to 1764 and 1691 $cm^{-1}$ (newly formed maleimide group in the five-membered ring), indicated successful imidization of PSMA into the PSMI derivative [32,33]. The absence of the C = O absorption bands of PSMA in the infrared spectrum of PSMI showed that complete conversion was achieved as substantiated by elemental analysis (Table 3) and $^{13}C$ NMR results (Fig. 1). Also shown are the typical overlapping absorption bands in the fingerprint area (1400–1500 $cm^{-1}$) and at 1599 $cm^{-1}$, associated with the C–H bending and C = C stretching vibrations of styrene, respectively [33].

#### 3.1.4. Electron microscopy and surface area analyses

The particle size and morphology of the PSMI nanoparticles in the dispersion as well as in the solid-state were investigated using transmission and scanning electron microscopy. Fig. 3 shows the TEM image and the corresponding size distribution histogram of the functionalized nanoparticles existing in the stable, opaque, aqueous dispersion.

The particle size distribution was somewhat bimodal with a small fraction of particles in the 65–72 nm range. Overall, uniform nanoparticles with spherical morphology were attained (Fig. 3). The average diameter of the nanoparticles was 50 ± 0.05 nm. It was possible to generate the PSMI nanoparticles reproducibly with particle sizes in the range 45–55 nm. Fig. 4 shows the SEM image and corresponding size distribution histogram of the dried PSMI scavenger particles after

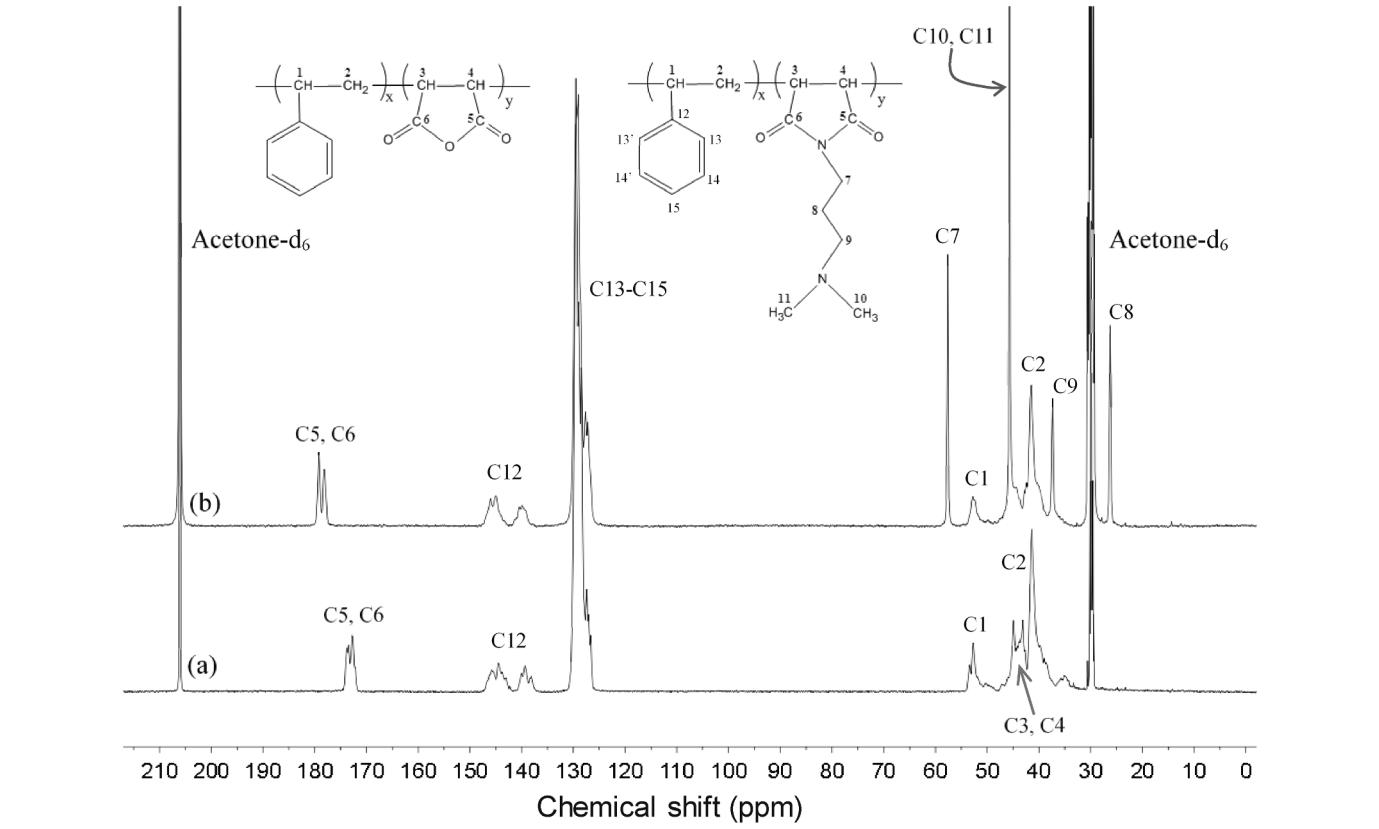



**Fig. 1.** Carbon-13 NMR spectra of (a) PSMA polymer and (b) PSMI scavenger in acetone. The chemical structures of the polymers with the carbon number allocations are shown as insets. Frequency: 150.586 MHz; Temperature: 317.9 K; Total acquisition time: 24 h. $^{13}C$ NMR chemical shifts were quoted relative to the acetone-$d_6$ resonance at 207 ppm.

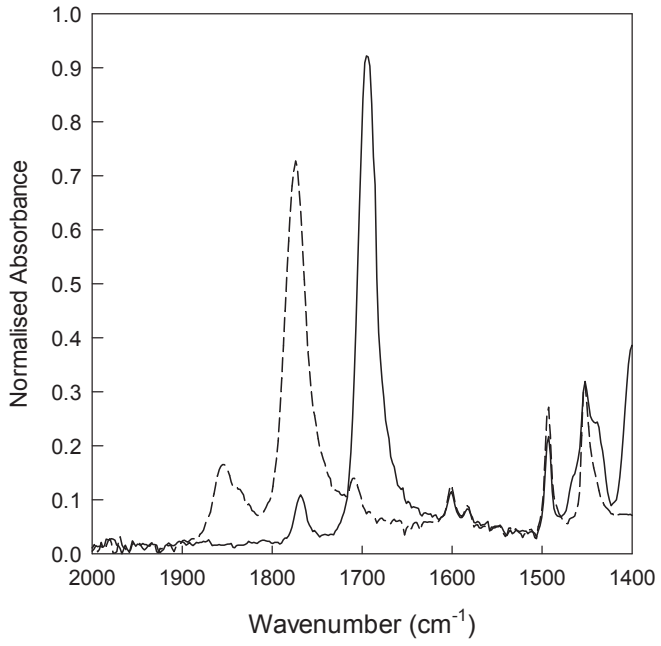



**Fig. 2.** FTIR spectra of the PSMA polymer (dotted line) and the PSMI scavenger (solid line).

isolation from the dispersion by freeze-drying.

The dried PSMI scavenger was composed of individual spherical nanoparticles with average particle sizes of 49.7 ± 0.02 nm, which was in excellent agreement with the average diameters obtained from the TEM analysis. This indicated that the integrity of the synthesized PSMI nanoparticles was retained when converting the product from dispersion form to the solid-state. The PSMI scavenger particles were found to have a specific surface area of 88.1 ± 2.2 $m^2/g$ (BET method). The moderately large surface-area-to-volume ratio along with the amine surface functionality of the scavenger particles allow for efficient and fast rate of Au (III) ions recovery from solution.

### 3.2. Adsorption and elution experiments

#### 3.2.1. Equilibrium adsorption isotherm

The equilibrium adsorption data, which represents the Au loading on the scavenger as a function of Au(III) ion concentration in the barren solution at equilibrium, is shown in Fig. 5.

The steep slope in the Au(III) barren concentration range 0–30 mg/L, indicated that the PSMI scavenger particles had a high affinity for Au(III) ions. At the conditions tested, the maximum experimental Au loading was 574 mg/g in equilibrium with 624 mg/L Au(III) in the barren solution. This is 574 g of Au loaded per kilogram of the scavenger or roughly 18.5 oz of adsorbed Au. At the current price range of Au bullion (US$1850 to US$2070 per ounce), this amounts to a revenue of US $34,225 to US$38,295 (based on the Au loading per kilogram of scavenger). The obtained Au equilibrium loading capacity can be attributed to the relatively large surface area offered by the nanoparticles and the reactive tertiary-amine functional groups.

Table 4 lists Au(III) adsorption capacities for different types of adsorbents with mostly amine functionality, including commercially available ion-exchange resins, laboratory-synthesized polymeric and inorganic materials. Key experimental conditions that influence the adsorption such as feed solution pH or acidity, shaking time, and reaction temperature are also shown. The shaking time indicated is the

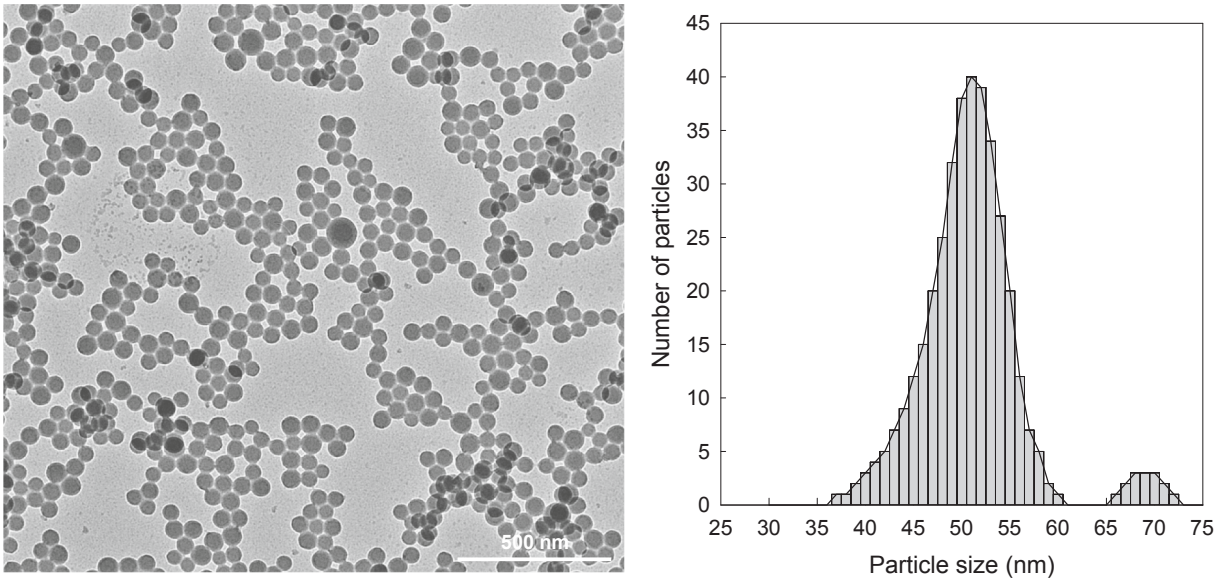



**Fig. 3.** TEM image of the PSMI scavenger nanoparticles and the corresponding particle size distribution histogram.

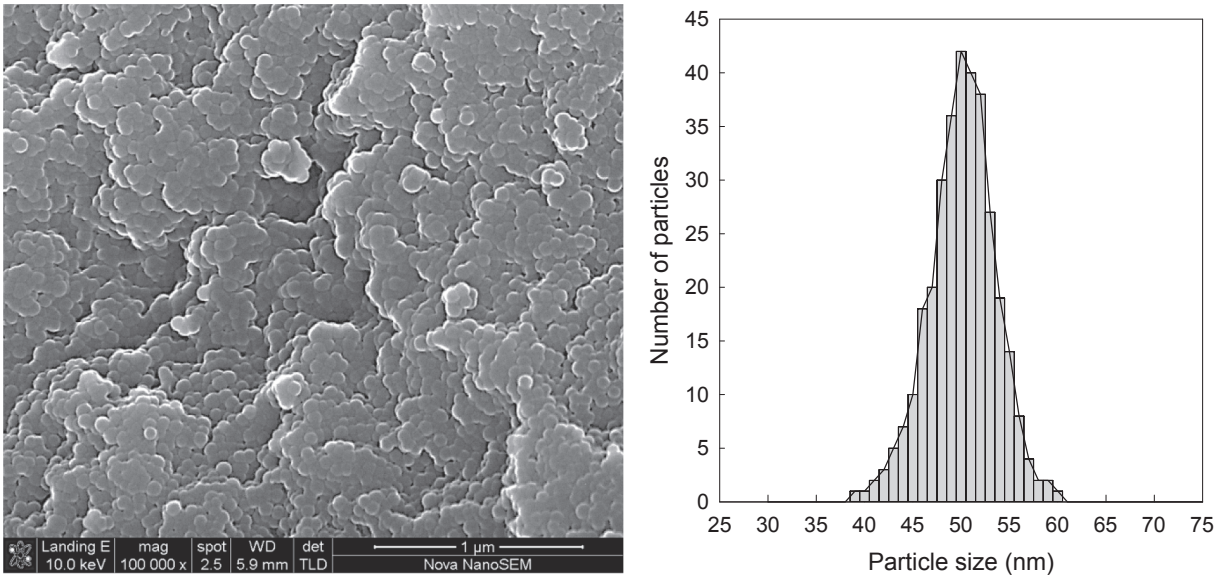



**Fig. 4.** SEM image of the PSMI scavenger nanoparticles (in solid-state) and the corresponding particle size distribution histogram.

contact time between adsorbent and Au(III)-bearing feed solutions to attain maximum uptake capacity. The equilibration time (given in parenthesis) is the time that was required to reach equilibrium as determined from kinetic studies. Table 4 indicates that the Au(III) loading obtained with our PSMI scavenger is comparable to adsorption capacities reported in the literature for EN-lignin (607 mg/g) [34] and *N*-methyl imidazole polystyrene beads (516 mg/g) [35] but is markedly higher than capacities obtained with commercial polymer-based resins Lewatit-MP64 (26 mg/g) [13] and Amberlite IRC 718 (136 mg/g) [36]. In their respective studies, Ohto *et al.* and Wang *et al.* reported very high loadings for Au of 906 mg/g at 30 °C and 6815 mg/g at 75 °C with their dimethylamine waste paper gel [9] and thioamide chelating nanofiber membranes [37]. These curiously high Au loading capacities were attributed to the chemical reduction of Au(III) to Au(0) on the adsorbent surfaces during adsorption, which created available binding site vacancies for further adsorption to occur.

Most papers in the public domain report on the recovery of Au(III) from dilute acidic solutions with pH values ranging from 1 to 6. Fewer papers report on the use of adsorbents for Au(III) recovery from highly acidic solutions. Authentic precious metal process liquors containing Au (III) ions will be highly acidic with pH values less than zero (or solution acidities >1 M HCl). To reach the reported Au(III) adsorption capacities of some of the listed adsorbents in Table 4, the pH of highly acidic process liquors will need to be adjusted with either buffer or caustic solutions which is costly and will dilute the aqueous Au(III) concentration further. Overshooting during pH adjustment can lead to unwanted localized Au(III) precipitation and Au losses. Other important considerations are the equilibration times and temperatures at which the adsorption takes place. Long equilibration and processing times delay the throughput and production of Au metal and temperatures higher than ambient conditions result in significantly higher energy costs since very large volumes of feed liquors will need to be heated-up to reach the optimum temperature. For some of the adsorbents in Table 4, high reaction temperatures of 45–75 °C and prolonged contact times of 2–3

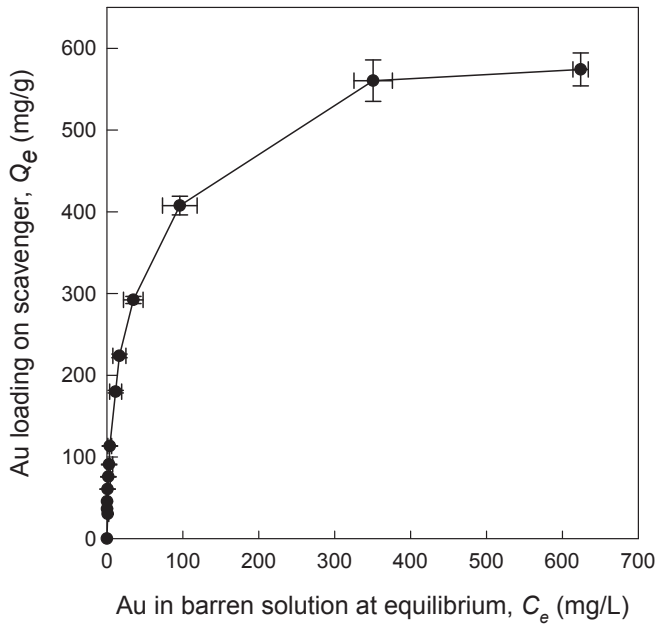



**Fig. 5.** Equilibrium Au(III) adsorption isotherm data of the PSMI scavenger. Initial Au(III) concentration in feed solution: 911 mg/L; Temperature: 25 ± 1 °C; Shaking time: 24 h.

days were required to attain the reported Au(III) loadings [8,9,35,37,39,40,43]. Therefore, the solution pH, contact time, and temperature, along with the cost of the adsorbent and downstream processing options, have a direct bearing on the economic and practical feasibility of the Au recovery process. Although the highest possible Au (III) adsorption capacity is desirable, a holistic approach incorporating all the above-mentioned factors must be evaluated when selecting an adsorbent and designing the recovery circuit. A trade-off must be made between Au(III) adsorption capacity, operational expenditure, revenue, and practicality. Our scavenger is cheap, requires short adsorption equilibration times (~5 min) and achieves consistently good Au loadings in a wide range of operating temperatures. As further results will demonstrate, the scavenger performs flawlessly in solutions with moderate to high acidities (0.1–5 M HCl), which makes them highly suitable for Au(III) recovery applications from real industrial process solutions. Moreover, a metal product can be isolated by disintegrating the polymer backbone of the scavenger.

To describe the Au(III) adsorption behavior onto the PSMI scavenger particles, the equilibrium adsorption data were fitted with the Langmuir, Freundlich, Redlich-Petersen, and Sips isotherm models as described in Table 5 [23–26].

The Langmuir and Freundlich isotherms contain two parameters, whereas the Redlich-Peterson and Sips isotherms are three-parameter models. Both the Redlich-Peterson and Sips models are combinations of the Langmuir and Freundlich models (Table 5), with some differences.

Fig. 6 shows the equilibrium adsorption isotherms for all four models together with the data points, and Table 6 shows the model parameters along with the calculated correlation coefficients according to Eq. (3).

Based on the correlation coefficient values, the Redlich-Peterson model fitted the experimental data well, but the Sips model represented the best fit of the experimental data and is therefore adequate for modeling the Au(III) adsorption process. This suggested that Au(III) loading onto the scavenger particles can be described by a combination of the Langmuir model (monolayer coverage with homogeneous binding sites) and the Freundlich model (multi-layer adsorption with heterogeneous binding sites). According to the literature, when the heterogeneity factor β in the Sips model is less than one, the adsorbent has more heterogeneous binding sites, and when β is about or equal to one, the

**Table 4**
Comparison of Au(III) adsorption capacities by different adsorbents reported in literature.

| Adsorbent | Solution pH or acidity | Shaking time (and equilibration time) | Maximum Au(III) uptake (mg/g) | Temperature (°C) |
|---|---|---|---|---|
| Amine modified divinylbenzene copolymers [38] | 1.00 | 48 h | 190 | 25 |
| *N*-methyl imidazole polystyrene beads [35] | 1.00 | 2 h | 516 | 45 |
| Ion-imprinted porous alginate microspheres [39] | – | 24 h (6 h) | 185 | 50 |
| Commercially available Amberlite IRC-718 resin [36] | 1.00 | 24 h | 136 | 25 |
| New metal organic polymer [40] | 2.00 | 48 h | 775 | 25 |
| Amine-phosphonic acid functionalized silica particles [27] | 2.00 | Not reported | 322 | 25 |
| Thioamide-group chelating nanofiber membranes [37] | 3.00 | > 4 h | 6815 | 75 |
| N-containing polymer particles [41] | 3.23 | 12 h | 1073 | 25 |
| Amine functionalized polystyrene nanoparticles [7] | 4.00 | Not reported (60 min) | 37.4 | 25 |
| Functionalized silica coated magnetite nanoparticles [28] | 5.00 | Not reported (240 min) | 286 | 45 |
| Novel lignin-based adsorption gels [8] | 0.5 M HCl | 100 h | 374–473 | 30 |
| Commercially available Lewatit-64 resin [13] | 1 M HCl | 750 min | 26.2 | 20 |
| Dimethylamine-modified waste paper [9] | 1 M HCl | 60 h (5 h) | 906 | 30 |
| Carbon prepared from barley straw and rice husk [11] | 1 M HCl | 24 h | 150 and 289 | 30 |
| Cellulose acetate fibers [42] | 2 M HCl | Not reported (1 h) | 110 | 25 |
| Pine bark tannin resin [43] | 2 M HCl | 72 h (>72 h) | 289 | 20 |
| **Poly(styrene-co-maleimide) nanoparticles (this study)** | **2 M HCl** | **24 h (5 min)** | **570** | **20–25** |

**Table 5**
Description of isotherm models for equilibrium adsorption.

| Isotherm model | Equation | Comments |
|---|---|---|
| Langmuir | $Q_e = Q_{e,max}k_LC_e/(1 + k_LC_e)$ | The model assumes monolayer adsorption. $Q_{e,max}$ is the maximum adsorption capacity predicted by the model at equilibrium and $k_L$ is the Langmuir constant [23] |
| Freundlich | $Q_e = k_FC_e^{1/n}$ | The model predicts multi-layer adsorption. $a_F$ and $b_F$ are empirical parameters, where $b_F$ is usually less than 1 [24]. |
| Redlich-Peterson | $Q_e = k_RC_e/(1 + a_RC_e^b)$ | This three-parameter model involves properties of both the Langmuir and Freundlich models. $k_R$ and $a_R$ are constants. The exponent $b$ lies between 0 and 1 [25]. |
| Sips | $Q_e = k_SC_e^\beta/(1 + a_SC_e^\beta)$ | At low ion concentration, this model reduces to the Freundlich model, and at high ion concentration, it predicts Langmuir behavior. $k_S$, $a_S$ *and* $\beta$ are parameters of the isotherm [26]. |

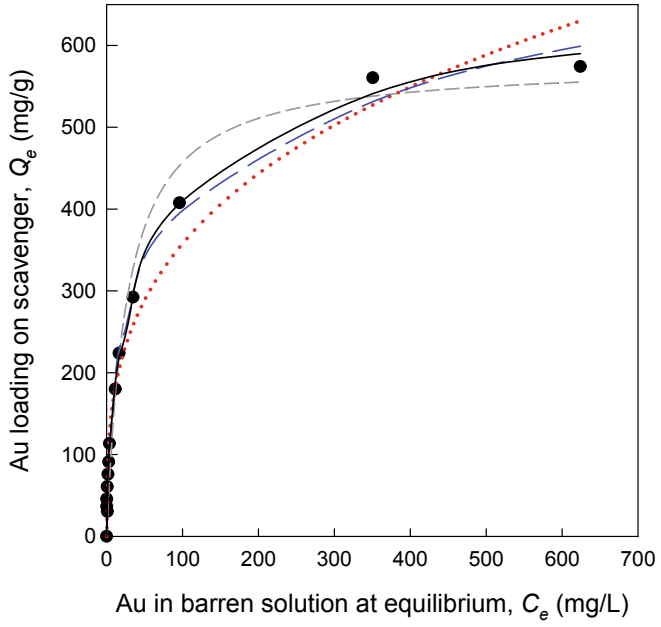



**Fig. 6.** Equilibrium Au(III) adsorption isotherm of the PSMI scavenger. Experimental data (●), Langmuir model (short dash line), Freundlich model (dotted line), Redlich-Peterson model (long dash line), Sibs model (solid line).

**Table 6**
Adsorption isotherm model parameters for Au(III) loading onto the PSMI scavenger.

| Isotherm model | Parameters† | Values |
|---|---|---|
| Langmuir | $Q_{e,max}$ (mg/g) | 579 |
| | $k_L$ (L/mg) | 0.038 |
| | $R^2$ | 0.986 |
| Freundlich | $k_F$ (mg/g) | 86 |
| | $N$ | 0.309 |
| | $R^2$ | 0.987 |
| Redlich-Peterson | $k_R$ | 60 |
| | $a_R$ | 0.340 |
| | $B$ | 0.807 |
| | $R^2$ | 0.995 |
| Sips | $k_S$ | 61 |
| | $a_S$ | 0.080 |
| | $B$ | 0.581 |
| | $R^2$ | 0.997 |

† All isotherm parameters, except $Q_{max}$, $k_L$ and $k_F$, are dimensionless.

adsorbent has more homogenous binding sites [24,44]. In the current work, the value of β was 0.581 which means that the PSMI scavenger nanoparticles presented sites predominantly heterogeneous in nature (Table 6).

The relationship between the percentage of Au recovery and Au loading onto the PSMI nanoparticles, as a function of the various scavenger-to-feed solution ratios (Table 1), is shown in Fig. 7.

For optimum Au loading on the scavenger (>560 mg/g), the scavenger-to-feed solution ratio must be less than or equal to one. However, if near-quantitative Au recovery (>98%) is targeted, a scavenger-to-feed solution ratio of greater than four is required. A compromise needs to be made, which depends on the aqueous Au(III) concentration and objective of the planned tests. For real-life applications, the higher loading capacity would be optimal, especially in counter-current continuous operations. In batch processes, higher recovery would be optimal, but there will be remaining functional groups for binding so the scavenger might not be fully utilized.

### 3.2.2. *Adsorption kinetics*

The rate of Au(III) adsorption by the scavenger, for shaking speeds of 50, 150, and 250 rpm, are shown in Fig. 8.

In all three scenarios, the rate of Au(III) uptake was extremely fast (Fig. 8). This was observed visually by an instantaneous color change of the Au(III) feed solution from yellow to pale and a corresponding change in color of the scavenger from white to a bright golden-yellow. After only 30 s, the Au loading achieved on the scavenger was 39.3, 40.1, and 40.6 mg/g for the kinetic tests done at 50 rpm, 150 rpm, and 250 rpm, respectively. After 3.5 min for the 250 rpm test, the Au loading on the scavenger reached equilibrium at 41.5 mg/g with a residual Au(III) concentration in the barren solution of 0.53 mg/L. This Au loading value agrees very well with the calculated Au loading capacity obtained from the equilibrium adsorption isotherm (Fig. 6). The Sips isotherm model (best description of the adsorption process), predicted the Au loading capacity of 40.1 mg/g in equilibrium with 0.53 mg/L Au(III) in the barren solution.

Kinetic models are often fitted to experimental data to identify the rate-controlling steps and to understand the mechanisms that govern the mass transfer of metal ions from the bulk solution to the sorption sites on the surface and inside the adsorbent particles, *i.e.* external and internal diffusion. In his paper, Simonin comprehensively explains that

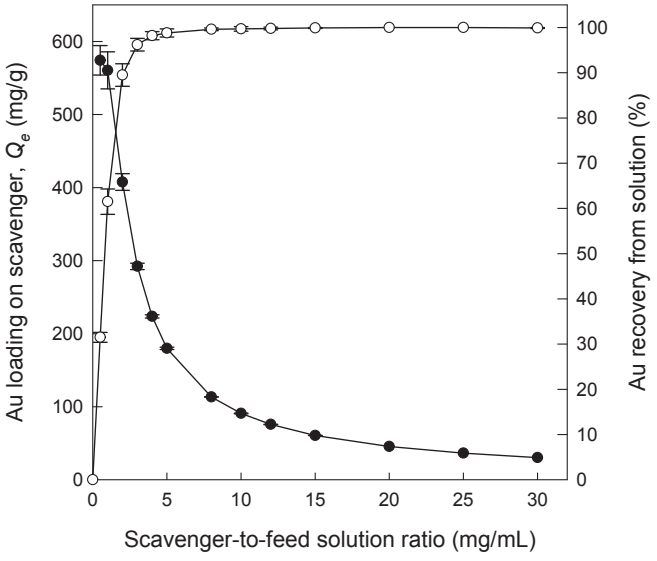



**Fig. 7.** The percentage of Au recovery (○) and the corresponding loading capacity of Au (●) versus scavenger-to-feed solution ratio (or scavenger dosage). Initial Au(III) concentration in feed solution: 911 mg/L; Temperature: 25 ± 1 °C; Shaking time: 24 h.

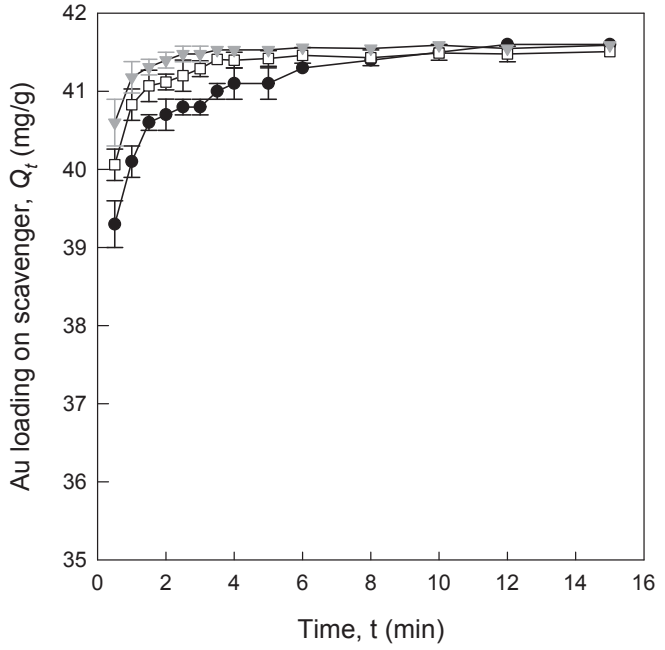



**Fig. 8.** The rate of Au(III) uptake by the scavenger at 50 rpm (●), 150 rpm (□), 250 rpm (▼). Initial Au(III) concentration in feed solution: 208 mg/L; PSMI scavenger dosage: 5 mg/mL; Temperature: 25 ± 1 °C.

experimental data at, or close to, equilibrium should not be included in the modeling of solid–liquid reaction kinetics [45]. The author states that taking data at equilibrium into account is not coherent and leads to incorrect modeling and interpretation of the adsorption kinetics. In our study, a significant number of experimental data points were near equilibrium (Fig. 8), and for that reason, kinetic models were not fitted to the data.

### 3.2.3. Adsorption thermodynamics

The Gibbs free energy was calculated from Eq. (5), while the change in enthalpy and the change in entropy were determined from the slope and intercept of a plot of ln $K_c$ versus 1/T (Eq. (7) (refer to Fig. S5 in the supplementary information section for the linear van't Hoff plot). The thermodynamic parameters are shown in Table 7.

The negative values of $\Delta G^0$ indicate that the Au(III) adsorption was spontaneous. The degree of spontaneity of adsorption increased with temperature (larger negative $\Delta G^0$ values), which can be attributed to chemisorption rather than physisorption [46]. Positive values of $\Delta H^0$ and $\Delta S^0$ indicate that the Au(III) ions uptake was endothermic between 283 and 313 K and that, during the process, randomness increased at the solid-solute interface [27–29]. The $\Delta H^0_{ads}$ value of 63.6 kJ/mol confirmed that the Au(III) adsorption onto the scavenger nanoparticles proceeded chemically because it falls in the 20.9–418.8 kJ/mol range [47]. Overall, the thermodynamic adsorption parameters reflect the high affinity of the PSMI scavenger towards Au(III) ions and the thermodynamic feasibility of the adsorption process.

**Table 7**
Thermodynamic parameters for the adsorption of Au(III) ions onto the PSMI scavenger.

| Temperature (K) | $\Delta G^0_{ads}$ (kJ/mol) | $\Delta H^0_{ads}$ (kJ/mol) | $\Delta S^0_{ads}$ (J/mol/K) |
|---|---|---|---|
| 283 | −9,331 ± 392 | 63.6 ± 7.2 | 257 ± 25 |
| 293 | −11,487 ± 272 | | |
| 298 | −13,187 ± 146 | | |
| 313 | −16,958 ± 412 | | |

### 3.2.4. Elution behavior

The elution efficiencies of the adsorbed Au species, with the different eluants listed in Table 2, are shown in Fig. 9.

The strongly acidic eluants of 3 M HCl (**EI**) and 6 M HCl (**EII**) were ineffective with less than 3% elution in each case. Elution tests with 3 M $HNO_3$/0.5 M HCl (**EIII**) and 6 M $HNO_3$/0.5 M HCl (**EIV**) showed an improvement in the elution with average elution efficiencies of 14% and 31%, respectively. The best results were obtained by an acidic solution of thiourea (**EV**), with an average elution of 75%. This higher extent of Au elution is attributed to highly favorable reactions between adsorbed Au species and thiourea to form stable cationic Au(I)-thiourea Au(SC$(NH_2)_2)_2^+$ complexes which are then released into the solution [10,13,23]. Increasing the thiourea content in the eluant solution did not improve the elution efficiency. It is believed that once Au(III) ions (as $AuCl_4^-$ complexes) are located at the surface of the scavenger particles after mass transfer, strong binding (electrostatic interaction and complexation) occurs with available protonated or unprotonated amine functional groups followed by electroless reduction of some adsorbed Au (III) species to both Au(I) and Au(0) species. The proposed Au(III) adsorption mechanism involving more than one surface chemical reaction and the heterogenous nature of the adsorption sites may explain the observed difficulty in elution of the adsorbed Au species. The spontaneous reduction of Au(III) species to Au(0) on adsorbent particle surfaces, resulting in poor elution, is not uncommon and has been reported in the literature for various other adsorbents [14,15,48].

### 3.2.5. Characterization of the Au-loaded scavenger with XPS, electron microscopy and PXRD

X-ray photoelectron spectroscopy (XPS) analysis was done to determine the oxidation states of the loaded Au species on the scavenger to gain insight into the incomplete elution processes. Fig. 10 shows the narrow scan XPS spectrum of a typical Au-loaded scavenger (*see* Fig. S6 in the supplementary information section for the survey scan XPS spectrum).

The Au 4f sub-peaks associated with contributions from Au species in different oxidation states of 0, +I, and + III are clearly distinguishable from one another within each region of the envelope (Fig. 10). Each sub-peak is split into two component peaks or doublets (Au $4f_{7/2}$ and Au $4f_{5/2}$) as a result of spin–orbit coupling. The binding energies (BE) of the Au $4f_{7/2}$ and Au $4f_{5/2}$ core levels together with the full width at half

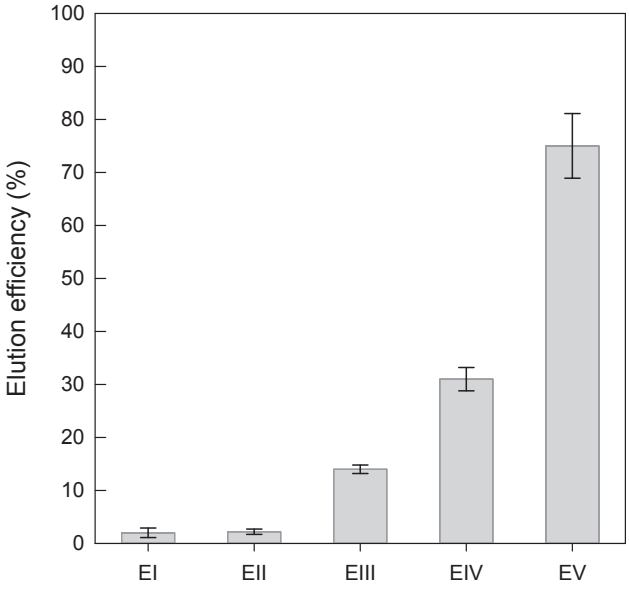



**Fig. 9.** Elution of adsorbed Au species from the Au-loaded scavengers with various eluants. Au-loaded scavenger dosage: 5 mg/mL; Temperature: 25 ± 1 °C; Shaking time: 24 h.

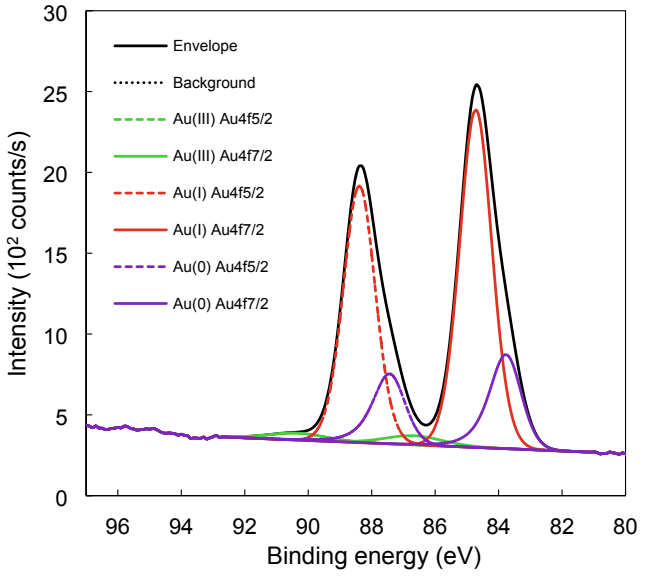



**Fig. 10.** Narrow scan XPS spectrum of the Au-loaded scavenger (loading ~ 90 mg/g) indicating the presence of Au(0), Au(I) and Au(III) species adsorbed on the scavenger particle surface.

maximum (FWHM) values and the quantification data of the loaded Au species are shown in Table 8.

The Au $4f_{7/2}$ component with binding energy at 83.8 eV is assigned to Au(0), presumably as small particles [49]. This is 0.2 eV lower than the typical value of 84.0 eV for metallic gold foil that is often used as an XPS reference material [50]. The Au $4f_{7/2}$ component with binding energy at 84.7 eV is attributed to Au(I) chloride surface species and linear $(AuCl)_n$ clusters, which agree reasonably well with analogous values reported in the literature of 84.7–85.1 eV for Au(I) sulfur surface species and for Au clusters with a binding energy of up to 84.7 eV [51,52]. The peak at 86.7 eV can be attributed to Au species in the highest oxidation state within the sample, most probably adsorbed trivalent Au(III) chloride species [53]. Assignments of Au oxidation states in the Au-loaded PSMI scavenger sample was further verified by comparison with practically identical Au4f peaks associated with Au(0), Au(I), and Au(III) species adsorbed onto solid nanocrystalline cerium oxide supports utilized as catalysts [54,55]. The FWHM values of the Au 4f peaks for Au(0) is ca. 1.0 eV, which is typical for bulk Au [49,56]. Shown in Fig. 11 are TEM images of an Au-loaded scavenger sample indicating the presence of adsorbed Au species on the surfaces of the PSMI nanoparticles.

Fig. 11 shows that the adsorbed Au species were present as a combination of highly dispersed ultra-small Au particles, intermediate-sized Au particles of 8–12 nm, and larger Au aggregates of 40–80 nm. It is likely that these variably sized Au particles and clusters represent the mixture of Au(0) (both small particles and bulk metal), Au(I), and Au (III) chlorides. Deconvolution of the respective areas under the peaks in Fig. 10 indicated that the adsorbed Au species was composed of 0.115 at. % Au(0), 0.439 at.% Au(I) and 0.021 at.% Au(III). Thus, the zero-valent Au(0) species amounted to 20% molar of the total Au present in the Au-loaded scavenger sample, and Au(I) and Au(III) species contributed ~ 76% and ~ 4%, respectively, to the total Au content of the sample.

**Table 8**
Summary of XPS analysis data for the Au-loaded PSMI scavenger.

| Adsorbed Au species | $Au4f_{7/2}$ | | $Au4f_{5/2}$ | | Au surface content | |
|---|---|---|---|---|---|---|
| | BE (eV) | FWHM (eV) | BE (eV) | FWHM (eV) | At.% | Molar % |
| 0 | 83.8 | 1.1 | 87.4 | 1.1 | 0.115 | 20.0 |
| +I | 84.7 | 1.2 | 88.4 | 1.2 | 0.439 | 76.3 |
| +III | 86.7 | 2.1 | 90.3 | 2.1 | 0.021 | 3.70 |

No apparent crystalline phases associated with finely divided colloidal Au(0) nanoparticles were detected in the Au-loaded scavenger sample with powder X-ray diffraction (PXRD) analysis (Fig. 12). For comparison, the adsorbed Au in the Au-loaded scavenger was subjected to reduction with a dilute solution of $NaBH_4$ for 2–3 min. In this case, crystalline colloidal Au(0) nanoparticles were detected by PXRD analysis and the reduced Au sample was purple [57]. In the solid-state bulk, Au is a yellow-colored metal, although it may be black, ruby, or purple when finely divided [58]. The PXRD diffractograms of the typical Au-loaded scavenger and of the sample consisting of reduced $Au^0$ on the Au-loaded scavenger are shown in Fig. 12.

Shown in Fig. 13 are photographs of (a) the fresh PSMI scavenger (without Au), (b) a typical yellow-colored Au-loaded scavenger sample, and (c) the Au-loaded scavenger sample after reduction with $NaBH_4$ solution. XPS analysis showed that the purple-colored sample consisted primarily of Au(0) (95.5%) and some Au(III) (4.5%).

### 3.2.6. *Metallic Au recovery from Au-loaded scavenger and mass balancing*

An alternative method for the complete recovery of Au directly from the Au-loaded scavengers was explored. The method entailed the complete digestion of Au-loaded scavenger samples, followed by selective reduction and precipitation of pure metallic Au with water. During the microwave digestion, the Au(0) species on the Au-loaded scavenger was probably oxidized to higher oxidation states by the nitric acid used as digestion matrix, and in the process, nitric acid decomposed. Fig. 14 shows optical microscope photographs of the Au flakes obtained, which had a characteristic golden-yellow metallic luster.

The metallic Au flakes were characterized by SEM-EDS analysis, and the micrograph is shown in Fig. 15. The metallic Au flakes had flower-like morphology, which consisted predominantly of elemental Au.

Table 9 shows the elemental mass balance accountability for three digestion-precipitation tests to recover difficult-to-elute adsorbed Au species from the Au-loaded scavenger. Also, shown in Table 9 are the quantity of Au loaded on the scavenger samples (mg Au per g of scavenger, and mg of Au adsorbed on scavenger) and the mass of metallic Au flakes recovered (in mg). Negligible concentrations of residual Au species were detected in the supernatant solution (*see* Scheme 2).

Some of the yellow metal flakes were lost through washing, filtration, and drying. Nonetheless, good Au elemental mass balance accountabilities were obtained between 95% and 100%.

The reduction reactions, leading to precipitation of metallic Au, can be explained in terms of thermodynamics with standard reduction potentials as shown in Eq. (11) to Eq. (13) [59].

$$Au^{3+} + 3\,e^- \rightleftharpoons Au \quad E^0 = 1.50\ V \tag{11}$$

$$Au^{+} + e^- \rightleftharpoons Au \quad E^0 = 1.69\ V \tag{12}$$

$$O_2 + 4H^+ + 4\,e^- \rightleftharpoons H_2O \qquad E^0 = 1.23\ V \tag{13}$$

According to Nicol *et al.* [59], because the standard reduction potential ($E^0$) for the $O_2$-$H_2O$ reaction (1.23 V) is lower than the values of 1.50 V for the $Au^{3+}$–Au reaction and 1.69 V for the $Au^{+}$–Au reaction, $Au^{3+}$ and $Au^{+}$ are thermodynamically unstable in water and will undergo spontaneous reduction to metallic Au with the oxidation of water to oxygen. The authors further stated that oxygen, with a standard reduction potential of 1.23 V, is not able to oxidize Au to $Au^{3+}$. The overall reduction reaction of $Au^{3+}$ and $Au^{+}$ in the digested solution (followed by precipitation) can be expressed by Eq. (14):

$$Au^{3+}{}_{(aq)} + Au^{+}{}_{(aq)} + 2\,H_2O_{(l)} \rightleftharpoons 2\,Au_{(s)} + 4H^{+}{}_{(aq)} + O_{2\,(g)} \tag{14}$$

Since the PSMI scavenger particles were prepared from cheap starting materials, this method of Au recovery by the destruction of the scavenger is an economically viable option. The value of the Au recuperated is orders of magnitude higher than the value of the scavenger itself. This represents a new approach of Au recovery without the need

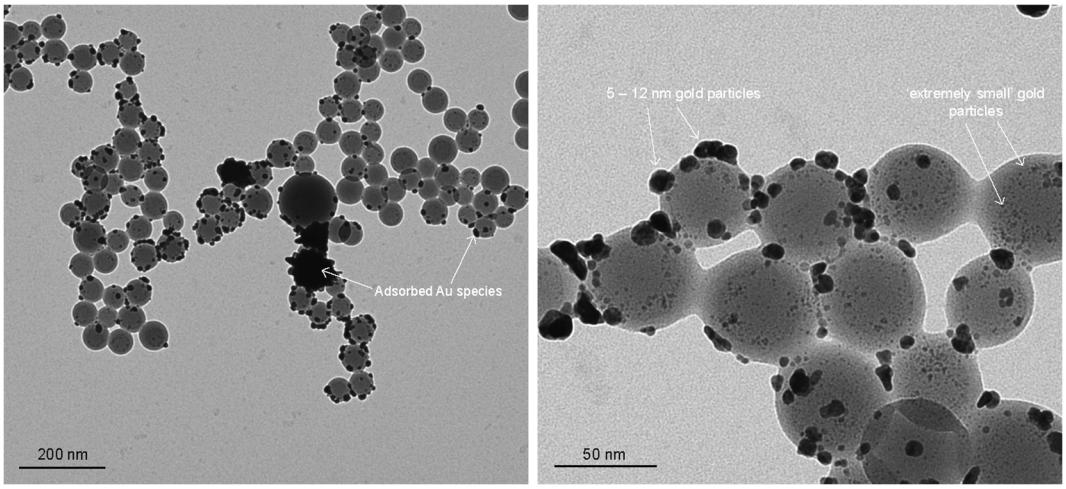



**Fig. 11.** TEM images of the Au-loaded scavenger nanoparticles indicating different sizes of adsorbed Au species (low and high magnification of the same sample).

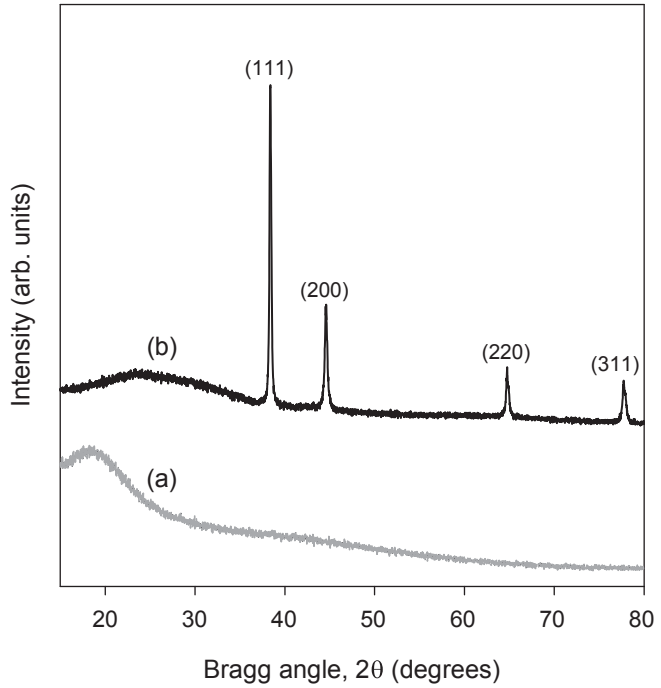



**Fig. 12.** PXRD diffractograms of (a) typical Au-loaded scavenger, (b) scavenger with reduced colloidal Au(0).

for unfavorable elution.

### 3.2.7. *Competitive adsorption behavior*

Although not the focus of this paper, tests were conducted to investigate the ability of the scavenger to recover Au(III) ions from acidic solution in the presence of co-existing metal ions and common counter anions. More specifically, we were interested to establish (1) whether the scavenger could bulk recover Au(III) ions and platinum group metal (PGM) ions from a mixed precious metal solution, (2) whether the scavenger in its current state and functionality offers any degree of selectivity towards Au(III) over other precious metal and heavy metal ions, and (3) whether chloride, nitrate and sulphate ions impede the Au(III) recovery. Fig. 16 shows the precious metal ion recovery. These noble metals are expected to be extracted as anionic chloro-complexes.

The order of recovery was Au(III) > Ir(IV) ≥ Pt(IV) ≥ Pd(II) ≫ Rh (III), under the experimental conditions tested. The scavenger was moderately selective for Au(III) ions over Ir(IV), Pt(IV), and Pd(II) ions, and highly selective over Rh(III) ions (refer to Table S3 in the supplementary information section for calculated selectivity coefficients). The poor recovery of Rh(III) can be ascribed to the extensive aquation of the $[RhCl_6]^{3-}$ ions in the solution, which strongly inhibits the adsorption of these complexes. The result in Fig. 16 is encouraging and suggests that bulk recovery of chloro-complex anions of Au(III) and PGMs is possible with the PSMI scavenger in its current form and amine functionality. Moreover, it appears that the scavenger is capable of separating Au(III), Ir(IV), Pt(IV), and Pd(II) from Rh(III) in solution, from which Rh(III) can be recovered more easily and effectively. At around US$21,800/oz, Rh is currently the most expensive of all the PGMs. More detailed research is

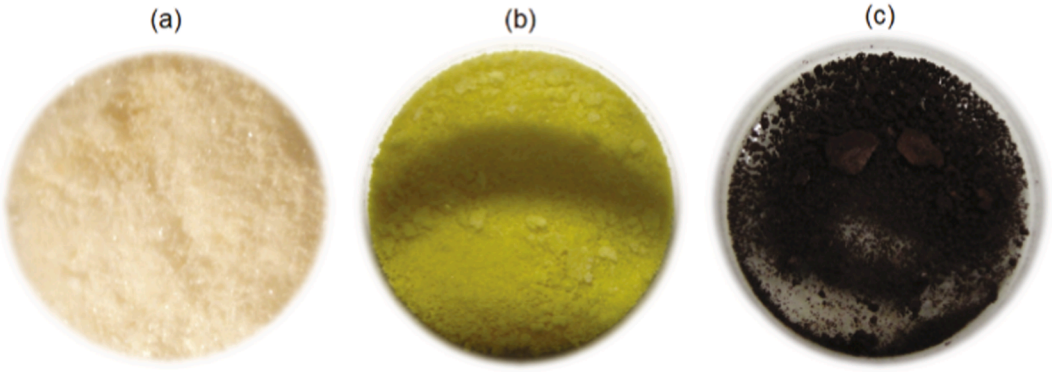



**Fig. 13.** Photographs of (a) the fresh scavenger, (b) a typical Au-loaded scavenger, and (c) scavenger material with reduced colloidal Au(0).

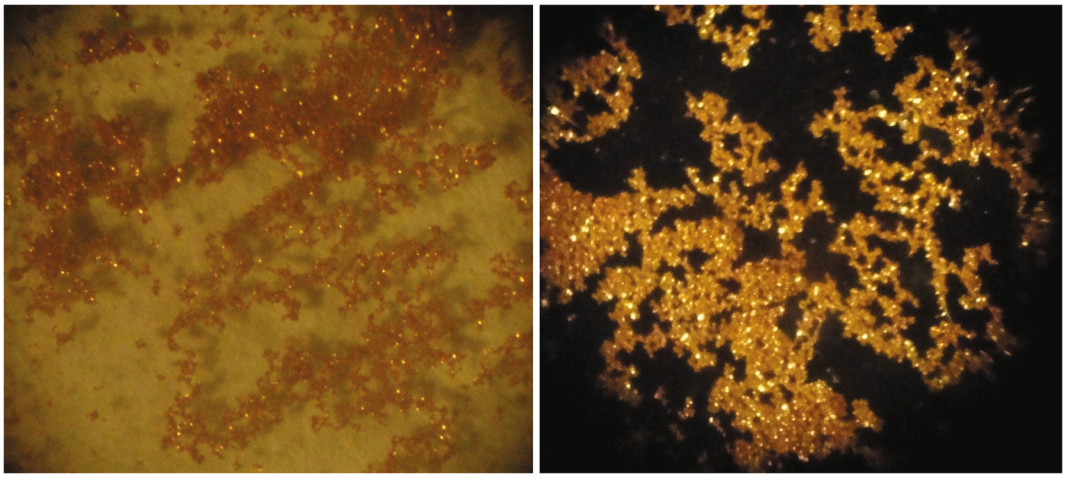


**Fig. 14.** Optical microscope photographs of the metallic Au flakes obtained by reduction and precipitation of dissolved Au species in the microwave digested liquor with water.

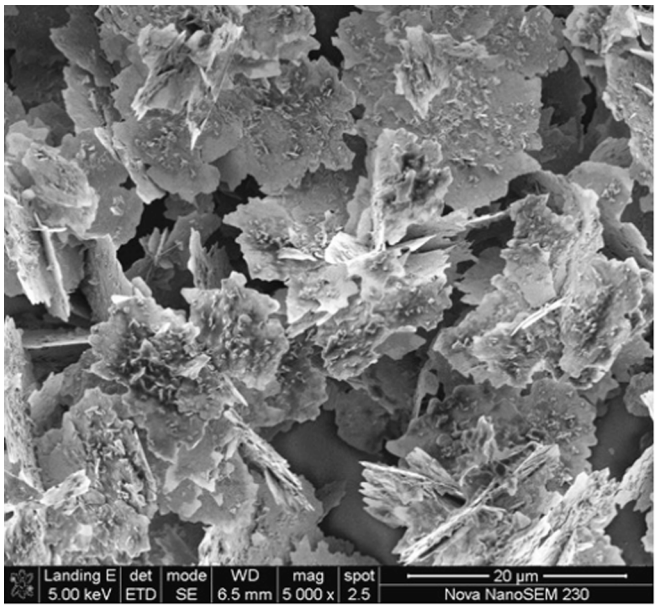



**Fig. 15.** SEM image of the recovered metallic Au flakes with flower-like morphology.

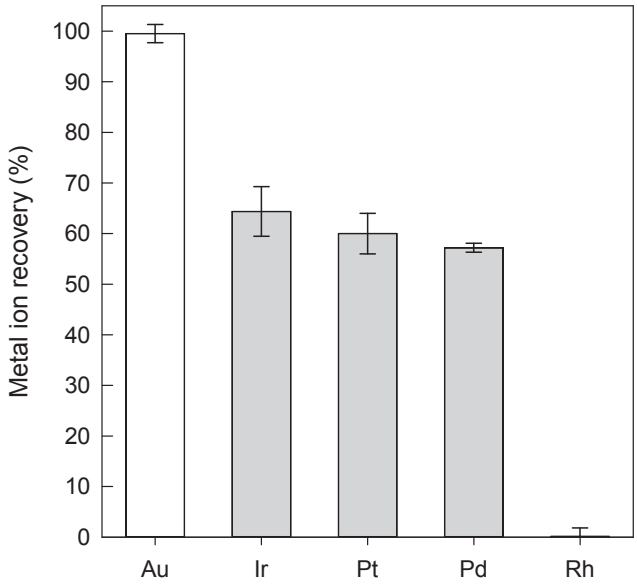



**Fig. 16.** Recovery of Au(III) from a mixed-metal solution containing other precious metals. Initial metal ion concentrations in the feed solution (2 M HCl matrix): Au(III) 21.2 mg/L, and Ir(IV), Pt(IV), Pd(II), Rh(III) ~ 50 mg/L; PSMI scavenger dosage: 5 mg/mL; Temperature: 25 ± 1 °C; Shaking time: 24 h.

**Table 9**
Elemental (Au) mass balance data for three Au-loaded PSMI scavenger samples.

| Au-loaded sample | Au loading† | Au loaded† | Precipitated Au | Accountability |
|---|---|---|---|---|
| | (mg/g) | (mg) | (mg) | (%) |
| 1 | 85.8 | 4.29 | 4.20 | 97.9 |
| 2 | 89.6 | 4.48 | 4.35 | 97.1 |
| 3 | 182 | 9.10 | 8.70 | 95.6 |

† Au loaded on the scavenger prior to digestion (calculated mass).

required, including a study of the metal ion speciation effects on the individual metal ion recoveries. If required, the functional groups of the PSMI scavenger can be tailored such to allow for selectivity of anionic Au(III) complex anions over the other anionic precious metal anions. Nonetheless, the PSMI particles appear to be a promising scavenger to bulk recover and preconcentrate valuable precious metal ions from acidic solution.

The recovery of Au(III) and heavy metal ions from acidic solution is shown in Fig. 17. Only the recovery efficiencies of Au(III), Ni(II), Fe(II), Cu(II) and Pb(II) are reported since Na(I), Mg(II) and Mn(II) were not extracted from the mixed-metal feed solution.

Fig. 17 shows that the scavenger is highly selective for Au(III) and very little or no adsorption of co-existing heavy metal ions occurred (refer to Table S4 in the supplementary information section for calculated selectivity coefficients). This is attributed to the fact that these heavy metals are typically present in solution as hydrated cationic complexes. As such, the metals were not preferentially loaded onto the PSMI scavenger since the mechanism underpinning the adsorption is electrostatic attraction between positively charged amine sites and $AuCl_4^-$. Some base metals, such as Zn(II), Cu(II), Pb(II) and Sn(IV), can form anionic chloro-complexes in equilibrium with their cations in highly acidic solutions. In the current work, it is plausible that Cu(II) and Pb(II) were somewhat co-extracted from solution as anionic complexes which competed with $AuCl_4^-$ ions for protonated amine binding sites on the scavenger nanoparticles. Similar selectivity observations of Au(III)

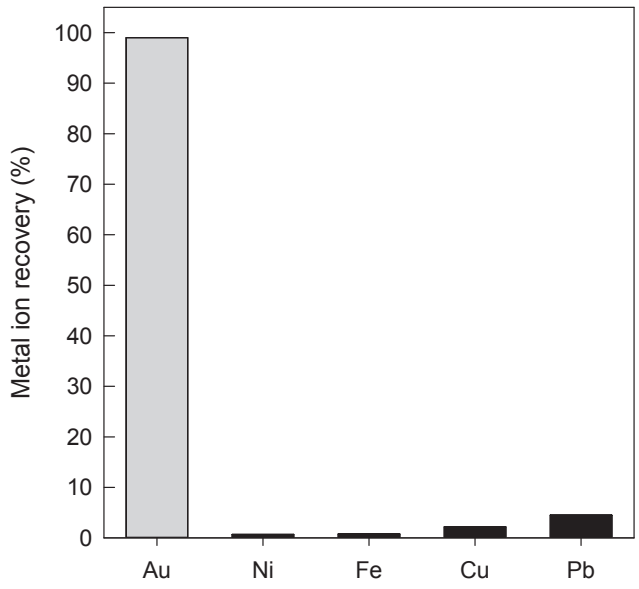



**Fig. 17.** Recovery of Au(III) from a mixed-metal feed solution containing heavy metal ions. Initial metal ion concentration in the feed solution (2 M HCl matrix): Au(III) ~ 143 mg/L, and ~ 300 mg/L Ni(II), Cu(II), Fe(II), Pb(II), Mg (II) and Mn(II); PSMI scavenger dosage: 5 mg/mL; Temperature: 25 ± 1 °C; Shaking time: 24 h.

over base metals have been reported by numerous studies in the literature [35,39,40,42,60].

Lastly, the effect of different concentrations of HCl and common anions (chloride, nitrate and sulphate) on the recovery of Au(III) ions was also studied. As shown in Table 10, the Au(III) recovery was basically unaffected by these constituents present in the feed solutions.

The selective recovery of Au(III) ions from acidic solutions containing background heavy metal ions, excess acid and common anions demonstrated that the scavenger is extremely versatile and can be applied in a range of process solutions.

## 4. Conclusions

Spherical tertiary-amine functionalized poly(styrene-*co*-maleimide) scavenger nanoparticles were successfully synthesized in a double-walled oil-heated autoclave using an organic solvent-free process. A detailed study on the recovery of Au(III) ions from acidic solution with the novel scavenger was undertaken. Langmuir, Freundlich, Redlich-Peterson, and Sips isotherm models were applied to analyze the experimental adsorption data. The best interpretation was given by the Sips isotherm model which indicated that Au(III) ion adsorption was a combination of monolayer and multi-layer sorption. A maximum Au loading of 574 mg/g was obtained and the Au(III) uptake by the scavenger occurred with extremely fast adsorption kinetics. The adsorbed Au species could only be partially eluted with acidified thiourea solution indicating very strong binding of Au species with the scavenger particles. The adsorbed Au species was however successfully recovered from the Au-loaded scavenger as metallic Au flakes using a scavenger-destruction and subsequent Au precipitation procedure as an alternative to elution. This eradicated the need for difficult and incomplete elution of adsorbed Au species, which maximizes resource recovery, saving time and costs, and it eliminates the environmental impact associated with spent acidic and thiourea eluant solutions. The metallic Au obtained can be sold directly to an off-taker such as a gold dealer or a refinery for refinement into a metal product of the desired specification. The fact that the scavenger is manufactured from inexpensive raw materials and that pure metallic Au is obtained makes this holistic approach of Au recovery an economically feasible process.

**Table 10**
Recovery of Au(III) from solution of various concentrations of HCl, NaCl, $NaNO_3$ and $NaSO_4$.

| Concentration (M) | HCl[†] | NaCl[§] | $NaNO_3$[§] | $NaSO_4$[§] |
|---|---|---|---|---|
| 0.1 | >98.4% | – | 98.4% | 99.0% |
| 0.2 | – | 99.4% | 99.3% | – |
| 0.5 | >98.8% | 99.1% | – | – |
| 1.0 | >99.0% | 98.9% | 99.1% | 99.2% |
| 2.0 | >98.9% | – | – | – |
| 3.0 | >99.2% | – | – | – |
| 5.0 | >98.0% | – | – | – |

[†] Feed liquor Au(III) concentrations ranging from 180 to 200 mg/L and scavenger dosages of 5 mg/mL.

[§] Feed liquor Au(III) concentration between 147 and 161 mg/L and scavenger dosages of 5 mg/mL. The feed liquor matrices were 2 M HCl in all cases, plus the respective dissolved salts with the different concentrations.

## Declaration of Competing Interest

The authors declare that they have no known competing financial interests or personal relationships that could have appeared to influence the work reported in this paper.

## Acknowledgments

The authors would like to thank the National Research Foundation (NRF, South Africa) and the National Fund for Scientific Research (F.R.S.-FNRS, Belgium) for financial support. BK acknowledges support by the South African Research Chairs Initiative of the Department of Science and Technology (DST) and NRF of South Africa (Grant No 46855). Madelaine Frazenburg (University of Stellenbosch) and Mohammed Jaffer (University of Cape Town) are kindly acknowledged for electron microscopy analyses and Pierre Eloy (UCLouvain) for assistance and useful discussions for XPS analyses. Polyscope (Geleen, the Netherlands) is also thanked for donating the PSMA copolymer used in this study.

## Appendix A. Supplementary data

Supplementary data to this article can be found online at https://doi.org/10.1016/j.cej.2021.128761.

## References

[1] [1] South Africa Gold Production 1990-2020. https://www.ceicdata.com/en/indicator/south-africa/gold-production (accessed June 30, 2020).
[2] [2] K. Gopaul, South African production: important but no longer globally significant, gold hub. (2019). https://www.gold.org/goldhub/gold-focus/2019/06/south-african-production-important-no-longer-globally-significant (accessed June 29, 2020).
[3] C.Y. Yap, N. Mohamed, An electronegative process for the recovery of gold from cyanide solutions, Chemosphere 67 (2007) 1502–1510.
[4] A. Ramesh, K. Fujiwara, T. Maki, H. Hasegawa, K. Ueda, Adsorption of platinum (IV), palladium(II) and gold(III) from aqueous solutions onto L-lysine modified crosslinked chitosan resin, J. Hazard. Mater. 146 (2007) 1–2.
[5] C. Gasparrini Gold and other precious metals: from ore to market 1993 Springer-Verlag.
[6] N.V. Nguyen, J. Jeong, M.K. Jha, J. Lee, K. Osseo-Asare, Comparative studies on the adsorption of Au(III) from waste rinse water of semiconductor industry using various resins, Hydrometallurgy 105 (2010) 161–167.
[7] K. Jainae, K. Sanuwong, J. Nuangjamnong, N. Sukpirom, F. Unob, Extraction and recovery of precious metal ions in wastewater by polystyrene-coated magnetic particles functionalized with 2-(3-(2-aminoethylthio)propylthio)ethanamine, Chem. Eng. J. 160 (2010) 586–593.
[8] D. Parajuli, C.R. Adhikari, M. Kuriyama, H. Kawakita, K. Ohto, K. Inoue, M. Funaoka, Selective recovery of gold by novel lignin-based adsorption gels, Ind. Eng. Chem. Res. 45 (2006) 8–14.
[9] C.R. Adhikari, D. Parajuli, H. Kawakita, K. Inoue, K. Ohto, H. Harada, Dimethylamine-modified waste paper for the recovery of precious metals, Environ. Sci. Technol. 42 (2008) 5486–5491.
[10] A. Ramesh, H. Hasegawa, W. Sugimoto, T. Maki, K. Ueda, Adsorption of gold(III), platinum(IV) and palladium (II) onto glycine modified crosslinked chitosan resin, Bioresour. Technol. 99 (2008) 3801–3809.
[11] R. Chand, T. Watari, K. Inoue, H. Kawakita, H.N. Luitel, D. Parajuli, T. Torikai, M. Yada, Selective adsorption of precious metals from hydrochloric acid solutions

using porous carbon prepared from barley straw and rice husk, Miner. Eng. 22 (2009) 1277–1282.
[12] K.F. Lam, C.M. Fong, K.L. Yeung, G. McKay, Selective adsorption of gold from complex mixtures using mesoporous adsorbents, Chem. Eng. J. 145 (2008) 185–195.
[13] F.J. Alguacil, P. Adera, M. Alonso, Processing of residual gold(III) solutions via ion exchange, Gold Bull. 38 (2005) 9–13.
[14] N.V. Nguyen, J. Jeong, D. Shin, B. Kim, J. Lee, B.D. Pandey, Simultaneous recovery of gold and iodine from the waste rinse water of the semiconductor industry using activated carbon, Mat. Trans. 53 (2012) 760–765.
[15] N.T. Santos, R. Landers, M.G.C. da Silva, M.G.A. Vieira, Adsorption of gold ions onto sericin and alginate particles chemically crosslinked by proanthocyanidins: a complete fixed-bed column study, Ind. Eng. Chem. Res. 59 (2020) 318–328.
[16] [16] K. Ziegler-Skylakakis, Concise International Chemical Assessment Document 49, Thiourea. (2003). https://www.who.int/ipcs/publications/cicad/en/cicad49.pdf?ua=1 (accessed July 02, 2020).
[17] M. Ahokas, C. Wilén, Synthesis of poly(styrene-co-maleimide) and poly (octadecene-co-maleimide) nanoparticles and their utilization in paper coating, Prog. Org. Coat. 66 (2009) 377–381.
[18] P. Samyn, D. Van Nieuwkerke, G. Schoukens, D. Stanssens, L. Vonck, H. Van den Abbeele, Synthesis of imidized nanoparticles containing soy oil under various reaction conditions, Eur. Polym. J. 66 (2015) 78–90.
[19] M. Daraie, M.M. Heravi, N. Sarmasti, Synthesis of polymer-supported Zn(II) as a novel and green nanocatalyst for promoting click reactions and using design of experiment for optimization of reaction conditions, J. Macromol. Sci. 57 (2020) 488–498.
[20] W.J. Cloete, L. Verwey, B. Klumperman, Permanently antimicrobial waterborne coatings based on the dual role of modified poly(styrene-co-maleic anhydride), Eur. Polym. J. 49 (2013) 1080–1088.
[21] W. Rasband, In Image J: Image processing and analysis in Java http://rsb.info.nih.gov/ij/ (2006).
[22] S.R. King, J. Massicot, A.M. McDonagh, A straightforward route to tetrachloroauric acid from gold metal and molecular chlorine for nanoparticle synthesis, Metals 5 (2015) 1454–1461.
[23] H.M.F. Freundlich, Over the adsorption in solution, Z. Phys. Chem. 57A (1906) 385–470.
[24] I. Langmuir, The constitution and fundamental properties of solids and liquids, J. Am. Chem. Soc. 38 (1916) 2221–2295.
[25] O. Redlich, D.L. Peterson, A useful adsorption isotherm, J. Phys. Chem. 63 (1959) 1024.
[26] R.J. Umpleby, S.C. Baxter, Y. Chen, R.N. Shah, K.D. Shimizu, Anal. Chem. 212 (2001) 4584–4591.
[27] W. Liu, P. Yin, X. Liu, X. Dong, J. Zhang, Q. Xu, Thermodynamics, kinetics, and isotherms studies for gold(III) adsorption using silica functionalized by diethylenetriaminemethylenephosphonic acid, Chem. Eng. Res. Des. 91 (2013) 2748–2758.
[28] N.F.A. Razak, M. Shamsuddin, S.L. Lee, Adsorption kinetics and thermodynamics studies of gold (III) ions using thioctic acid functionalized silica coated magnetite nanoparticles, Chem. Eng. Res. Des. 130 (2018) 18–28.
[29] M. Mihăilescu, A. Negrea, M. Ciopec, C.M. Davidescu, P. Negrea, N. Duţeanu, G. Rusu, Gold (III) adsorption from dilute waste solutions onto Amberlite XAD7 resin modified with L-glutamic acid, Sci. Rep. 9 (2019) 8757.
[30] Y. Inoue, A. Nishioka, R. Chûjô, Carbon-13 nuclear magnetic resonance spectroscopy of polystyrene and poly-α-methylstyrene, Macromol Chem Phys 156 (1972) 207–223.
[31] N.T. Hieu Ha, Determination of triad sequence distribution of copolymers of maleic anhydride and its derivatives with donor monomers by 13C n.m.r. spectroscopy, Polym. J. 40 (1999) 1081–1086.
[32] M. Ahokas, C. Wilén, Modified and functionalized maleimide copolymers for paper coatings, Polym Bull 66 (2011) 491–501.
[33] D.L. Pavia, G.M. Lampman, G.S. Kriz, Introduction to Spectroscopy, 3rd ed., Harcourt College Publishers, New York, U.S.A, 2001.
[34] D. Parajuli, H. Kawakita, K. Inoue, M. Funaoka, Recovery of gold(III), palladium(II) and platinum(IV) by aminated lignin derivatives, Ind. Eng. Chem. Res. 45 (2006) 6405–6412.
[35] X. Kou, B. Ma, R. Zhang, M. Cai, Y. Huang, Y. Yang, Properties and mechanism for selective adsorption of Au(III) on an ionic liquid adsorbent by grafting N-methyl imidazole onto chloromethylated polystyrene beads, RSC Adv. 10 (2020) 20338–20348.
[36] C.I. Park, J.S. Chung, K.W. Cha, Separation and preconcentration method for palladium, platinum and gold from some heavy metals using Amberlite IRC 718 chelating resin, Bull. Korean Chem. Soc. 21 (2000) 121–124.
[37] X. Li, C. Zhang, R. Zhao, X. Lu, X. Xu, X. Jia, C. Wang, L. Li, Efficient adsorption of gold ions from aqueous systems with thioamide-group chelating nanofiber membranes, Chem. Eng. J. 229 (2013) 420–428.
[38] D. Jermakowicz-Bartkowiak, B.N. Kolarz, A. Serwin, Sorption of precious metals from acid solutions by functionalized vinylbenzyl chloride-acrylonitryle-divinylbenzene copolymers bearing amino and guanidine ligands, React. Funct. Polym. 65 (2005) 135–142.
[39] X. Gao, J. Liu, M. Li, C. Guo, H. Long, Y. Zhang, L. Xin, Mechanistic study of selective adsorption and reduction of Au(III) to gold nanoparticles by ion-imprinted porous alginate microspheres, Chem. Eng. J. 385 (2020).
[40] W. Xu, X. Mo, S. Zhou, P. Zhang, B. Xiong, Y. Liu, Y. Huang, H. Li, K. Tang, Highly efficient and selective recovery of Au(III) by a new metal-organic polymer, J. Hazard. Mater. 380 (2019).
[41] S. Zhou, W. Xu, C. Hu, P. Zhang, K. Tang, Fast and effective recovery of Au(III) from aqueous solution by a N-containing polymer, Chemosphere 260 (2020).
[42] J. Yang, F. Kubota, Y. Baba, N. Kamiya, M. Goto, Application of cellulose acetate to the selective adsorption and recovery of Au(III), Carbohydr. Polym. 111 (2014) 768–774.
[43] M.B.Q.L.F. Torrinha, H.A.M. Bacelo, S.C.R. Santos, R.A.R. Boaventura, C.M. S. Botelho, Uptake and recovery of gold from simulated hydrometallurgical liquors by adsorption on pine bark tannin resin, Water 12 (2020) 3456.
[44] W.S.W. Ngah, S. Fatinathan, Adsorption of Cu(II) ions in aqueous solution using chitosan beads, Chem. Eng. J. 143 (2008) 62–72.
[45] J.P. Simonin, On the comparison of pseudo-first order and pseudo-second order rate laws in the modelling of adsorption kinetics, Chem. Eng. J. 300 (2016) 254–263.
[46] M.E. Argun, S. Dursun, M. Karatas, M. Gürü, Activation of pine cone using Fenton oxidation for Cd(II) and Pb(II) removal, Bioresour. Technol. 99 (2008) 8691–8698.
[47] L. Deng, Y. Su, H. Su, X. Wang, X. Zhu, Sorption and desorption of lead(II) from wastewater by green algae Cladophora fascicularis, J. Hazard. Mater. 143 (2007) 220–225.
[48] X. Huang, Y. Wang, X. Liao, B. Shi, Adsorptive recovery of Au3+ from aqueous solutions using bayberry tannin-immobilized mesoporous silica, J. Hazard. Mater. 183 (2010) 793–798.
[49] E.T. Kang, Y.P. Ting, K.G. Neoh, K.L. Tan, Electroless recovery of precious metals from acid solution by N-containing electroactive polymers, Synth. Met. 69 (1995) 477–478.
[50] M.J. Scaini, G.M. Bancroft, S.W. Knipe, An XPS, AES, and SEM study of the interactions of gold and silver chloride species with PbS and FeS2: Comparison to natural samples, Geochim. Cosmochim. Acta 61 (1997) 1223–1231.
[51] M.J. Scaini, G.M. Bancroft, S.W. Knipe, Reactions of aqueous Au1+ sulfide species with pyrite as a function of pH and temperature, Am. Min. 83 (1998) 316–322.
[52] S.B. Di Cenzo, S.D. Berry, E.H.J. Hartford, Photoelectron spectroscopy of single size Au clusters collected on a substrate, Phys. Rev. B 38 (1988) 465–468.
[53] S.K. Bhargava, F. Mohr, J.D. Gorman, Oxidative addition reactions of methyl substituted binuclear gold complexes studied by X-ray photoelectron spectroscopy, J. Organomet. Chem 67 (2000) 93–96.
[54] A. Abad, P. Concepción, A. Corma, H. Garcia, A collaborative effect between gold and a support induces the selective oxidation of alcohols, Angew. Chem. Int. Ed. 44 (2005) 4066–4069.
[55] Q. Fu, H. Saltsburg, M. Stephanopoulus, Active nonmetallic Au and Pt species on ceria-based water-gas shift catalysts, Science 301 (2003) 935–938.
[56] N. Bogdanchikova, A. Pestryakov, M.H. Farias, J.A. Diaz, M. Avalos, J. Navarrete, Formation of TEM- and XRD-undetectable gold clusters accompanying big gold particles on TiO2-SiO2 supports, Solid State. Sci. 10 (2008) 908–914.
[57] N.N. Long, L.V. Vu, C.D. Kiem, S.C. Doanh, C.T. Nguyet, P.T. Hang, N.D. Thien, L. M. Quynh, Synthesis and optical properties of colloidal gold nanoparticles, J. Phys.: Conf. Ser. 187 (2009) 187 012026.
[58] New World Encyclopedia. (2017). https://www.newworldencyclopedia.org/entry/Gold (accessed July 12, 2020).
[59] M.J. Nicol, R.L. Paul, C.A. Fleming, The chemistry of the extraction of gold, chapter 15, Southern African Institute of Mining and Metallurgy, Conference, Johannesburg (1987) 831–905.
[60] S. Zhou, X. Mo, W. Zhu, W. Xu, K. Tang, Y. Lei, Selective adsorption of Au(III) with ultra-fast kinetics by a new metal-organic polymer, J. Mol. Liq. 319 (2020).